Design of an ON-OFF closed loop Deep Brain Stimulator for Parkinson's Disease and Essential Tremor

BY

ISHITA BASU
B.S., Jadavpur University, India, 2005
M.S., University of Illinois at Chicago, 2010

THESIS

Submitted as partial fulfillment of the requirements
for the degree of Doctor of Philosophy in Electrical and Computer Engineering
in the Graduate College of the
University of Illinois at Chicago, 2012

Chicago, Illinois

Dissertation Committee:

Daniela Tuninetti, Chair and Advisor
Daniel Graupe, Co-advisor
Rashid Ansari
Konstantin V Slavin, Neurosurgery
Daniel M Corcos, Kinesiology

To my parents, Dr Amitabha Basu and Dr Bharati Basu.

ACKNOWLEDGMENTS

I would like to express my deepest gratitude to my advisors Dr. Daniela Tuninetti and Dr. Daniel Graupe as well as Dr. Konstantin Slavin for giving me an opportunity to work in this project and for their constant guidance and support. I would like to thank Dr. Daniel Corcos for helping me immensely with EMG data recording as well as helping me understand some of the basics in the EMG study. I would also take this opportunity to thank Dr. Leo Verhagen Metman and Dr. Slavin who helped me recruit patients from their clinics as well as understand some of the intricate details associated with the patient population. I would also want to thank Dr. Rashid Ansari for helping me with some of the EMG signal processing.

A special thanks to all the study subjects, without whom nothing would have been possible. I would like to thank everyone in the Neural Control of Movement Laboratory, specially Dr. Fabian Jude David, Dr. Cynthia Poon and Dr. Julie A. Robichaud for helping me with the data collection and my colleague, Pitamber Shukla for helping me with some aspects of the EMG study. I would also like to thank all the staff in the ECE department for helping me with numerous administrative issues and making my stay comfortable. Last but not least, I would like to thank my parents, husband and friends for their constant encouragement and support throughout the past six years.

IB

TABLE OF CONTENTS

TABLE OF CONTENTS (Continued)

CHAPTER **PAGE**

LIST OF TABLES

LIST OF TABLES (Continued)

TABLE **PAGE**

LIST OF FIGURES

LIST OF FIGURES (Continued)

LIST OF FIGURES (Continued)

FIGURE **PAGE**

LIST OF ABBREVIATIONS

PD	Parkinson's Disease
ET	Essential Tremor
DBS	Deep Brain Stimulation
STN	Subthalamic Nucleus
OUP	Ornstein Uhlenbeck Process
IG	Inverse Gaussian
ISI	Inter-Spike Interval
FPT	First Passage Time
sEMG	surface-Electromyography
acc	acceleration
WT	Wavelet Transform
PP	Poisson Process
HFS	High Frequency Stimulation
VIM	Ventral Intermediate Nucleus
LFP	Local Field Potential
SNR	Signal to Noise Ratio

SUMMARY

This thesis examines the feasibility of building the next generation of deep brain stimulation (DBS) protocol by developing the theoretical aspect behind modifying the existing stimulation paradigm to overcome some of its shortcomings. This innovative technology is based on closed-loop ON-OFF control of DBS using physiological signals measured from patients with pathological tremor. The main objectives are as follows:

- Model the neuronal dynamics at the DBS target. This model can be used to determine optimal stimulation parameters for the DBS-ON period.
- Design an algorithm using non-invasively measured physiological signals, to predict an impending tremor during the DBS-OFF period .

DBS is a surgical treatment involving the implantation of electrodes and a pacemaker, which sends electrical impulses to specific parts of the brain (1). DBS in select brain regions has provided remarkable therapeutic benefits for otherwise treatment-resistant movement and affective disorders such as Parkinsons Disease (PD), Essential Tremor (ET), chronic pain and dystonia (2). Despite the long history of DBS (3), its underlying principles and mechanisms are still not clear. DBS directly changes brain activity in a controlled manner and its effects are reversible (unlike those of lesioning techniques). The Food and Drug Administration (FDA) approved DBS as a treatment for ET in 1997, for PD in 2002, and for dystonia in 2003. DBS is also routinely used to treat chronic pain and has been used to treat various affective disorders, including major depression. The FDA approved DBS systems operate open-loop, i.e., the

physician sets the stimulation parameters with visual feedback from the patient. Stimuli are provided continuously and stimulation parameters remain constant over time.

This thesis concentrates on using neuronal, surface-EMG (sEMG) and acceleration (acc) signals recorded from PD and ET patients for designing an adaptively controlled ON-OFF DBS system. The results would however have far reaching implications on the treatment of a number of neurological and behavioral conditions such as depression, chronic pain, epilepsy, obsessive compulsive disorder, traumatic brain injuries, Alzheimer's disease, etc. which recently have been considered good candidates for DBS-type treatments where similar modeling techniques can be applied for adaptively controlling stimulation.

The thesis starts by introducing two major movement disorders, PD and ET that debilitate a considerable proportion of the population and how DBS has emerged as a popular surgical method in relieving them. It also includes some existing literature on the possible mechanisms underlying the therapeutic effects of DBS.

The second chapter deals with modeling of neuronal firing activity recorded from the affected areas of the brain, from patients undergoing surgery for DBS. A simple Ornstein-Uhlenbeck Process (OUP) is used to model the spike activity recorded from the subthalamic nucleus (STN) of PD patients and that from the ventral intermediate nucleus of the thalamus (VIM) of ET patients at the time of implantation of the electrodes for DBS. This model is shown to have superior performance in general than other simpler stochastic process models. A good predictive model of the neuronal activity can be used to simulate the neuronal membrane potential at the

DBS target which is not otherwise measurable and will thus help determine the effect of a range of DBS parameters on the simulated quantity of interest.

The third chapter introduces a modified model as described in chapter 2 to include the effects of stimulation parameters on the modeled neuronal dynamics. It also includes three possible metrics that can be used to assess the effect of different stimulation parameters on the neuronal dynamics. Some preliminary simulation results are presented based on two ET data sets.

The fourth chapter explores the possibility of using sEMG and acc signals for adaptive ON-OFF control of DBS. To achieve this, sEMG and acc signals recorded in ET and PD patients during and after DBS stimulation is analyzed. At the end of each stimulation period, there emerged a period when there is no tremor even with the stimulation off. Using a set of parameters extracted from the sEMG and acc signals, a prediction algorithm is designed. This allows predicting onset of tremors at end of the tremor-free DBS-OFF intervals and establishes the feasibility of noninvasive ON-OFF control of DBS in certain ET and PD patients. By adapting in real-time the DBS-OFF duration, we envisage that intermittent stimuli will achieve the same benefits of current non-adaptive continuous stimuli at a reduced level of injected electrical charge in the brain. This will (a) diminish brain over-stimulation, thus reducing the possibility of damage to healthy neurons and (b) lower power consumption, thus prolonging DBS battery life.

The thesis concludes by pointing out interesting directions of future work. On the long term, we envisage that our DBS technology based on closed-loop feedback control can be op-

erated wirelessly from the neuro-stimulator (that can now be worn as portable device) to the implanted electrode. This will eliminate the need to surgically implant the neurostimulator and connectiong wire to the electrodes, and will allow for an almost complete flexibility in adjusting, adapting and upgrading future DBS technologies.

CHAPTER 1

INTRODUCTION

Deep Brain Stimulation (DBS) is a form of treatment that uses a surgically-implanted battery-operated medical device that delivers high-frequency electrical stimulation (HFS) to targeted areas in the brain that control movement. The stimulation blocks the abnormal nerve signals that cause tremor either during voluntary movement (as in ET and PD) or during rest (as in PD) as well as other PD symptoms such as rigidity and akinesia. DBS underlying principles and mechanisms are not fully understood yet. However, unlike pre-DBS surgical techniques such as lesion surgery, DBS directly changes the brain activity in a controlled manner and its effects are reversible.

1.1 Parkinson's disease and DBS

Parkinson's disease (PD) is a progressive degenerative disorder of the central nervous system that impairs motor skills. The estimated prevalence is 0.3% in the whole population in industrialized countries, rising to 1% in those over 60 years of age and to 4% in the population over 80 (4). The main symptoms include tremor, rigidity, imbalance and slowness of movement. Parkinsonian tremor is generally a mild resting tremor with slow, regular oscillations of 4-6 Hz. It might also be present during posture or voluntary movements (postural/action tremor) which is typically in the 7-11 Hz frequency range. PD is caused by degeneration of cells in the basal ganglia, an area in the brain that controls movement, which leads to decreased levels of the

neurotransmitter, dopamine. The depletion of dopamine leads to abnormal synchronized firing of neuronal groups that oscillate at frequencies below 30Hz. These oscillations cause tremor and disrupt normal motor functions (5). Dopamine replacement therapy, using the dopamine precursor levodopa, is the mainstay of therapy in PD and is effective for many years. However, as the disease progresses, the response to each dose of levodopa shortens and becomes associated with excessive involuntary movements called dyskinesias (6). For these advanced PD patients a surgical procedure called deep brain stimulation (DBS) can provide significant benefit for all motor symptoms while reducing or eliminating dyskinesias and improving quality of life (5; 7). The Food and Drug Administration (FDA) approved DBS for PD in 2001.

1.1.1 Mechanisms and Effects of DBS

DBS underlying principles and mechanisms are still uncertain. Neurons within the globus pallidus (GPi) and the subthalamic nucleus (STN) in the basal ganglia system form a functional network that ordinarily in healthy subjects resonates at around 70 Hz (8). This is important for optimal organization of voluntary movement. With reduced dopamine levels, the STN/GP network seems to oscillate at frequencies below 30 Hz. These oscillations are related to tremor and are believed to disrupt normal motor functions. Neurons directly affected by DBS would thus represent a barrier for the transmission of synchronized low frequency oscillations throughout the basal ganglia network.

DBS is thought to *mask* the underlying activity of neurons surrounding the electrode, independent of their original mode of operation (9; 10). This masking can result from either a suppression of intra-neuronal activity (5) or from a locking of the firing to the stimulus fre-

quency (8). It is further hypothesized that DBS produces a pattern of excitation and inhibition in the entire basal ganglia network that depends on a number of factors, such as the frequency of excitation, the excitation location, the distance of the cell from the stimulating electrodes, etc (11; 12; 13; 14). The mechanism of excitation or inhibition produced might not be the same for all the neurons. Both the inhibition and excitation actually lead to a single effect on the basal ganglia neurons: *disrupting* the existing pattern in the basal ganglia network (5). It is still uncertain what disrupts the disruption. The disruption could be achieved by inhibiting the existing deleterious synchronization pattern which is like a noisy signal to the brain. This would imply that the absence of a noisy signal from which the brain possibly cannot decode any information is better than its existence. The disruption could also be caused by a new firing pattern superimposed to the noisy one. This new firing pattern is not due to the network interactions but due to the constant external stimulation. In either case, the firing patterns of neurons directly affected by DBS are no longer regulated by their network interactions, but instead by the continuous and unchanging stimulation (15).[1]

1.2 Essential Tremor and DBS

Essential Tremor (ET) is a progressive neurological disorder characterized by a rhythmic tremor (4-12 Hz) that is present only when the affected muscle is exerting effort and can be in the arms, head (neck), jaw and voice as well as other body regions (16). ET is the most

---

[1]General therapeutic stimulations parameters for DBS are (13): amplitude: 1-5 V, (square wave) pulse duration: 60-200 micro-seconds, and frequency: 120-180 Hz. Frequency is the most important parameter. It has been shown that stimulation in the 120-180 Hz range is useful, stimulation in the 10-50 Hz range does not produce improvement, while stimulation in the 5-10 Hz range worsens PD symptoms.

common movement disorder, with a prevalence of approximately 4% in persons over age 40 and about 5% among those over age 60 (17). The incidence of ET is approximately ten times that of PD. The pathophysiology of ET is not known. However, clinical, physiological and imaging studies point to an involvement of the cerebellum and/or cerebello-thalamocortical circuits (18). More specifically, ET is thought to arise from oscillatory activity within a central network or cell group that becomes unregulated, allowing spinal reflex loop oscillations. It has also been proposed that stretch loop circuits may become unstable and drive muscle contractions to produce tremor as in ET (19). There is no cure for ET, but there are treatments that give relief and improve quality of life. These include drug therapies such as propranolol and primidone (20) and surgical procedures. If the tremor is severely disabling and drugs do not relieve the symptoms, surgery may be an option. Two types of surgery used to treat ET are DBS (21) and thalamotomy (22). In thalamotomy, a lesion is placed on a small part of the thalamus and is irreversible. In DBS, an electric probe is placed in the Ventral Intermediate Nucleus (VIM) of the thalamus which is connected to a pacemaker placed near the collarbone. It stimulates the thalamus with pulses of electricity, which are thought to block the brain activity that causes tremor, and is reversible. However, the mechanisms of DBS and its beneficial effects on ET patients are not well understood.

1.3 Current Open-Loop DBS system

A DBS system consists of three components: the lead, the extension, and the neurostimulator. The lead is a thin insulated wire/electrode implanted in the brain. The lead contains 4 thin insulated electrodes whose tips are positioned within the targeted brain area (electrodes 0, 1,

2, 3). The neurostimulator, similar to a cardiac pacemaker, is implanted under the skin below the collarbone or over the abdomen. The extension is an insulated wire that is passed under the skin and connects the lead to the neurostimulator. Once the system is in place, electrical impulses are sent from the neurostimulator up along the extension wire and the lead and into the brain. The preferred target sites in the brain for placement of stimulating electrodes are the internal segment of the globus pallidus (GPi) and the subthalamic nucleus (STN) for PD patients depending on the dominant symptoms, and ventral intermediate nucleus (VIM) of the thalamus for ET patients.

The only FDA approved DBS system for PD/ET is manufactured by Medtronic, Inc. Their Activa system operates *open-loop.*The Activa system has 4 electrodes per lead, with their exposed contacts separated by 0.5 mm. In monopolar stimulation mode, the case of the pulse generator is the anode and one or more of the 4 electrodes can be the cathode(s); in bipolar stimulation mode, the cathode(s) as well as the anode(s) are provided by the electrodes. The clinician chooses the optimal electrode combination and sets the stimulation parameters (pulse amplitude, duration and frequency). DBS programming is based on subjective and objective clinical observations to ensure that the patient receives maximal benefit and minimal side effects. DBS is provided continuously over time and the stimulation parameters remain constant over time until the next visit of the patient to the clinician. Thus, the current DBS technology is neither adaptive to the patients' needs nor to the patients' disease progression over time.

1.4 Next Generation Closed-Loop DBS system

In order to adapt to the patients' condition, current DBS systems must be redesigned so as to include a closed-loop feedback control where the patients' symptoms are continuously monitored and the stimulation is adapted in response to its variations. To design an adaptively controlled closed-loop DBS system, it is necessary to find a suitable physiological signal that can be easily measured and has predictive information on tremor reappearance once DBS is OFF. One such feedback signal could be the actual neuronal brain activity measured from individual neurons (micro-recording) represented by the cell firing, or a group of neurons (macro-recording) represented by the local field potential, at the site where the DBS electrodes are implanted. However, the measurement of these signals by means of DBS electrodes (during DBS-OFF times) requires changes to the current FDA approved DBS system. Such a neuronal activity-based closed-loop DBS system would then require long testing and approval times thus delaying its commercialization. Alternatively, muscular activity measured by means of surface-electromyogram (sEMG) and accelerometer (acc) signals can be recorded non-invasively from the patient's symptomatic extremities. These signals are known to carry predictive information on tremor reappearance (23) and hence can be used for adaptive closed-loop ON-OFF control of DBS.

1.5 Goals, merits and impacts

The main goal of this dissertation is to provide the proof of principle for the next generation of *closed-loop* DBS systems. Our innovative approach markedly differ from current DBS

technology: it is based on time-adaptive, closed-loop control of the DBS-OFF duration based on signals measured in real-time from PD and ET patients.

We challenge the prevailing open-loop paradigm for two main reasons:

1. Delivering short packets of HFS just before PD/ET symptoms are predicted to reappear has the same beneficial effects of high-frequency continuous stimulation but at a much lower cost in terms of electrical current injected in the brain;
2. DBS can be used to treat pathologies that do not present clear visible symptoms, such as tremor or slowness in movements. For those diseases, it is imperative to be able monitor in real-time the brain response to electrical stimulation, to adapt the stimulation to the brain's ever changing conditions and drive its response to match the desired healthy one.

Any open-loop technology is doomed to fall short of achieving these two ambitious goals.

In order to design a closed-loop ON-OFF DBS system, the following goals were set:

1. Develop an accurate yet simple mathematical model of the area of the brain that controls movements;
2. Verify the mathematical modeling assumptions by using signals measured from PD and ET patients at the time of implantation of the DBS electrodes;
3. Extract features from real-time measured signals such as sEMG and acc that correlate with the beneficial effect of DBS and use them to predict the reappearance of tremor during the DBS-OFF period.

This novel closed-loop DBS technology will minimize the devices' power requirements, thus prolonging battery life as well as diminish over stimulation of the brain cells surrounding the electrodes, thus reducing the possibility of destroying healthy cells. The potentials of the findings of this research however go well beyond advancing treatments for pathological tremor suppression. They have the potential to extend to a number of neurological and behavioral conditions which are thought to benefit from DBS-type electrical stimulation, and thus will serve humanity in the long-term.

1.6 Summary of the contributions

1. A simple stochastic model (OUP) was fitted to the neuronal activity measured from the DBS target in patients with PD and ET.
2. The goodness of fit was quantified and compared with other simpler stochastic models. The OUP model performed better in general than the others used for comparison. Thus the OUP can indeed serve as a simple model for spike generation in the STN and VIM neurons of PD and ET patients respectively.
3. A simple way of including the effect of stimulation parameters in the OUP model was proposed and some simulation results based on the modified model showed that it can be used to determine an optimal set of stimulation parameters.
4. sEMG and acc measured non-invasively from tremor affected muscles of ET and PD patients were shown to contain predictive information that can be used to design a tremor prediction algorithm.

This forms the basis of designing an adaptively controlled ON-OFF DBS system. The proposed sEMG/acc based tremor predictor can be used as an add-on sub-system for the FDA-approved DBS system by leveraging the currently available telemetry capabilities of DBS [1]. Indeed, the external sEMG/acc sensors and the implanted neurostimulator can exchange data through the existing telemetry/wireless link.

[1]Medtronic DBS system comprises a device called the physician programmer through which a clinician can adjust DBS parameters and transmit these changes via radio telemetry to the implanted neurostimulator.

CHAPTER 2

MODELING OF NEURONAL ACTIVITY IN THE ABSENCE OF EXTERNAL STIMULATION IN PARKINSON'S DISEASE AND ESSENTIAL TREMOR PATIENTS

The contents of this chapter has been published in biological cybernetics (24) and in the proceedings of the 32nd Annual International Conference of the IEEE Engineering in Medicine and Biology Society (25)

2.1 Background and motivations

The brain consists of neuronal clusters densely interconnected in complex ways. These interconnections are not fully understood yet. Neuron clusters form groups by means of bidirectional and/or unidirectional connections. Synchronized firing between clusters is thought to be one form of signaling used by the brain to perform correlated tasks (26). However, in certain movement disorders neuronal clusters within particular loops are rhythmically active in an abnormal way (8; 27) causing pathological tremor. The three commonest forms of pathological tremor are parkinsonian tremor, essential tremor, and cerebellar intention tremor. The distinctive neurophysiological pathways for these tremors have been surprisingly difficult to decipher (28).

In PD, the death of dopaminergic nigrostriatal neurons causes abnormal neuronal oscillations in the loop linking the cortex, basal ganglia, and thalamus (28). Levy et al. (29) showed that an increase in synchronization between neurons in the basal ganglia contributes to the clinical features of PD. Synchronized neuronal oscillatory activity may severely impair normal brain functions. Several studies indicate that PD resting tremor (3-7Hz) is caused by a cluster of neurons located in the STN that fire synchronously at a frequency close to that of the tremor (27; 30; 31; 32). Under normal conditions, these neurons would fire incoherently. In particular, synchronous activities between pairs of neurons in the globus pallidus and in the substabtia nigra in patients with limb tremor at tremor frequency (3-7Hz) and in the beta range (15-30Hz) was reported (29). Depth recordings from PD patients by Weinberger et al. (33) demonstrated coherence between neuronal discharge and local field potential (LFP) in the beta range (15-30Hz), thus confirming that beta range oscillatory activity in the STN is dramatically increased in PD and may interfere with movement execution. In light of these studies, it is conjectured that DBS alleviates PD symptoms by disrupting the low-frequency synchronized oscillatory activity of the basal ganglia network.

A sizeable body of experimental data indicates enhanced olivocerebellar oscillation as a possible pathophysiology behind ET, even though necropsies have revealed no abnormalities (34). Lesions in the cerebellum and thalamus (35) greatly reduce ET, which suggests that abnormal oscillation is transmitted to the motor cortex via the cerebellum and its projection to the ventrolateral thalamus. The ventrolateral thalamus has abundant reciprocal connections with the motor and supplementary motor cortex, and functional MRI studies have shown

activation of the motor cortex in patients with ET (36). However, it was reported that there was no tremor-related coherence between the cortical magnetoencephalogram (MEG) and the EMG of contralateral fingers in six patients with ET (37). This finding however does not imply that the primary motor cortex is not involved in generation or maintenance of ET. Failure to find significant coherence between MEG and EMG could be due to inadequate sensitivity of the former or to inadequate sampling of the affected muscles (28). Intraoperative recordings typically reveal tremor-correlated oscillation in about 30% of all ventrolateral thalamic neurons (38) which indicates that only small subpopulations of oscillating thalamic neurons are involved in the tremor of a particular muscle at any given time. Hellwig et al. (39) showed that using simultaneous EEG-EMG recordings, there was significant corticomuscular coherences at the tremor frequency in ET. The results suggest that the sensorimotor cortex is involved in the generation of ET, in a similar way to that previously shown in parkinsonian resting tremor (40).

The pathophysiology of PD, ET, and cerebellar intention tremor affects different parts of the motor system, but the collective rhythmicity of widely distributed neuronal networks seems to be necessary for the clinical expression of tremor. The thalamocortical loop may not be the main site of oscillation in ET, but may simply facilitate tremor through neuronal entrainment (the drawing of additional cortical neurons into oscillation) and reverberation. Similarly, the basal ganglia could be the principal source of oscillation, as hypothesized for PD, or might also promote oscillation that is generated elsewhere (28).

The lack of fundamental understanding of the pathophysiology behind generation of tremor and other symptoms in PD and ET is reflected in the absence of a good predictive mathematical

model of the neuronal activity in the affected areas (STN, thalamus). Such a model would shed light into the mechanisms, and thus the beneficial effects of DBS in alleviating PD and ET symptoms in patients (41). The model parameters extracted from the measured data could be used as an indicator of the pathological state of the patient. In particular, their time variation would be related to the re-appearance of symptoms when DBS is stopped. By predicting the effect of DBS parameters, such as the amplitude, frequency, and waveform shape, the model parameters would serve as an index for optimizing DBS parameters (42; 26; 43; 44; 45). An optimal DBS would adapt to each and every individual patient's need and administer electrical stimuli to the brain only when actually needed. Hence, a good mathematical model that captures the system dynamics responsible for the generation of neuronal signals in the affected brain regions, which at the same time is not too complex to be of practical use, is indeed a prerequisite to designing the next generation of DBS systems.

2.1.1 Selecting a model

There have been numerous efforts in modeling either a single or a group of neurons, from the simple Hodgkin-Huxley model to mimic a single neuron (46), to complex neural networks for modeling a network of neurons (47). These computational models involve a large number of parameters and require an accurate and detailed *microscopic* knowledge of the interactions among all the neurons involved (48). One desirable approach is to develop a *macroscopic* model for a neuron and a neuron cluster that does not rely on the microscopic detailed knowledge of all possible interactions between neurons. Since neurological data is highly stochastic in nature, stochastic models of neuronal activity are a natural choice. Stochastic models have several

advantages over their deterministic counterparts: they involve lesser parameters and are robust to uncertainty in the exact parameter values (49).

Several linear stochastic models, with various degrees of complexity, have been proposed to model the neuronal activity from different parts of the human brain. One of the earliest stochastic models for neuronal spiking used in neurophysiology is the Poisson Process (PP) (50; 51). A PP has a simple mathematical description in terms of a single parameter that represents the average inter-spike interval. Unfortunately, the PP does not capture the mechanism of a spike generation (52). It has also been reported that a log-normal distribution fits better the measured inter-spike interval histograms than the exponential distribution resulting from a PP (53). A Wiener Process (WP) has also been used to model neuronal spiking (52). The main advantage of the WP is that the inter-spike interval distribution has a simple closed form expression which is the inverse gaussian distribution. Unfortunately, the WP does not predict the exponential decay in the membrane potential in between two subsequent input impulses to the neuron. An even more general point process model for neural spiking activity (54) requires the estimation of 28 parameters.

Nonlinear stochastic processes have also been used to model a group of neurons (26) where the neurons are modeled as coupled phase oscillators driven by random forces. Although well posed, Tass' model (26) suffers from the drawback of a difficult parameter extraction problem since the neuronal cluster phase is difficult to estimate from measured data.

Neuronal dynamics has also been modeled as a chaotic system (55). Sarbaz et. al (56) proposed that signals obtained from a healthy person have a chaotic nature while in the patho-

logical condition, the system is less chaotic nature and DBS restores the chaotic nature thus ameliorating disease symptoms. This approach could be potentially used for modeling of aggregate activity such as LFP and sEMG.

In this chapter, a simple Ornstein Uhlenbeck Process (OUP) (57) is considered for modeling the spiking activity of neurons in the STN and VIM of thalamus. The OUP was first proposed as a model for the neuronal potential dynamics in (58) and is now widely accepted (59; 60) because it has many advantages over simpler stochastic models, namely:

a) it accounts for the spike generation mechanism,

b) it predicts the exponential decay in the membrane potential in between two subsequent input impulses to the neuron,

c) it only involves the specification of two parameters along with a third free parameter , and

d) the two model parameters can be easily identified from measured data.

The OUP thus strikes a balance between an oversimplified model, such as the PP (50), and more complicated models (54; 26). However, the OUP might not model satisfactorily every type of neuronal activity in different parts of the brain (61). The model parameters of the OUP are identified from the recorded neuronal data that contains information about the spike times of a single neuron. The fit of the proposed model to the measured data is then assessed by quantifying its capacity of predicting the inter spike interval distribution. The model is also compared with two other simpler stochastic models.

2.2 The Orsnstein Uhlenbeck Process as a model of neuronal firing activity

The neuronal activity as recorded from the STN/thalamus consists of neuronal spikes (action potentials) produced by a single cell with superimposed background aggregate activity of neurons in the vicinity and measurement noise. The spike times provide information about the inter-spike interval (ISI) distribution of the neuron while the background activity is the membrane potential of a group of neurons surrounding the electrode's measuring tip, which is essentially the time varying aggregate input to the neuron. Here, an Orsnsten Uhlenbeck process (OUP) was used to model the membrane potential across a single neuron. When the membrane potential exceeds a certain threshold, the neuron fires. Thus, the spike times, or equivalently the ISIs, are related to the level crossing problem of the membrane potential process.

2.2.1 The Ornstein-Uhlenbeck Process

The OUP is a stochastic process, X_t governed by the following Langevin equation:

$$dX_t = (\mu - (X_t/\theta))dt + \sigma dW_t, \tag{2.1}$$

where $\theta > 0$, μ and $\sigma > 0$ are the model parameters, and W_t denotes the standard Wiener process, i.e., dW_t is a zero-mean white Gaussian process with variance dt. The parameter $\mu\theta$ represents the equilibrium or mean value; σ represents degree of volatility around the mean; $1/\theta$ represents the rate by which the volatility dissipates and the variable reverts towards the mean. In the OUP, the drift term $(\mu - (X_t/\theta))$ depends on the current value of the process X_t as opposed to the classical Wiener process where the drift is constant. This fact has the

following implication: if the current value of the process X_t is less than the mean $\mu\theta$, the drift $(\mu - (X_t/\theta))$ is positive and the process is "pushed-up" towards the mean. On the other hand, if the current value of the process is larger than the mean, the drift is negative and the process is "pushed-down" towards the mean. This feature is the reason why the OUP is known as the "mean reverting" process.

The Langevin equation in (Equation 2.1) can be solved using Ito's lemma (62; 63) with function $f(X,t) = Xe^{t/\theta}$, thus giving

$$df(X,t) = \mu \mathrm{e}^{t/\theta} dt + \sigma \mathrm{e}^{t/\theta} dW_t. \tag{2.2}$$

By integrating (Equation 2.2) from 0 to t and by multiplying both sides by $\mathrm{e}^{-t/\theta}$ we get:

$$X_t = \mu\theta + (x_0 - \mu\theta)\mathrm{e}^{-t/\theta} + \sigma \int_0^t \mathrm{e}^{-(t-s)/\theta} dW_s, \quad t \geq 0, \tag{2.3}$$

where x_0 is the value of X_t at time $t = 0$.

Let $f_{OU}(x,t)$ denote the probability density function of X_t in Equation 2.3, that is, $f_{OU}(x,t)$ is the probability that at time t the random variable X_t has value arbitrarily close to x. The Fokker-Planck equation that governs the dynamics of the distribution $f_{OU}(x,t)$ is given by:

$$\frac{\partial f_{OU}(x,t)}{\partial t} = \frac{1}{\theta} \frac{\partial \left\{ (x - \mu\theta) f_{OU}(x,t) \right\}}{\partial x} + \frac{\sigma^2}{2} \frac{\partial^2 f_{OU}(x,t)}{\partial x^2}. \tag{2.4}$$

The analytical solution of Equation 2.4 can be obtained by using a Fourier transform (60) and is given by:

$$f_{OU}(x,t) = \sqrt{\frac{1}{\theta[1-\mathrm{e}^{-2t/\theta}]\,\pi\sigma^2}} \cdot \exp\left\{\frac{-[(x-\mu\theta)-(x_0-\mu\theta)\mathrm{e}^{-t/\theta}]^2}{[1-\mathrm{e}^{-2t/\theta}]\,\theta\sigma^2}\right\}, \quad t \geq 0. \tag{2.5}$$

The time dependent distribution in Equation 2.5, in the limit for $t \to \infty$ has a Gaussian distribution of mean $\mu\theta$ and variance $\theta\sigma^2/2$ as stationary distribution, that is,

$$f_{OU}(x,\infty) = \sqrt{\frac{1}{\pi\theta\sigma^2}} \exp\left\{\frac{-(x-\mu\theta)^2}{\theta\sigma^2}\right\}. \tag{2.6}$$

A process like the OUP in Equation 2.1 can be assumed to be responsible for the spike generation in a single neuron model, as is described in (59; 60). Indeed, the state of a neuron can be described by a random variable X_t, representing the variation of the potential difference across its membrane. Let x_0 be the resting potential of the membrane, and θ be the membrane's time constant. In the absence of any input, X_t spontaneously decays to $\mu\theta$ according to Equation 2.3 with $\sigma = 0$. Consider now a dendritic input that consists of sequences of Poisson distributed impulses that can be excitatory or inhibitory with rates α_e and α_i, respectively. Let there be p excitatory input dendrites and q inhibitory input dendrites and for simplicity we assume that the input impulse rate for each dendrite is the same. The membrane potential X_t changes by e or i depending on the type of input, that is

$$X_{t+dt} = X_t + e, \quad e > 0,$$

for excitatory impulse and

$$X_{t+dt} = X_t + i, \quad i < 0,$$

for inhibitory impulse.

It can be shown (59) that the transition density function of the membrane potential can be described by an OUP with parameters θ given by the membrane's time constant and $\mu = p\alpha_e e + q\alpha_i i; \sigma = \sqrt{p\alpha_e e^2 + q\alpha_i i^2}$.

2.2.2 The First Passage Time problem

In order to identify the model parameters in (Equation 2.1), a sample path of the process is required. That is, recordings of the intracellular membrane potential without any other superimposed "background activity" signal is required. The background activity will be referred to as noise in the rest of the chapter. With *in vivo* extra-cellular recording, it is not possible to obtain a noise-free signal. The model parameters in Equation 2.1 can still be identified by using information about the spike timings available from the extracellular single neuronal activity recording, which is described in more details in Section 2.4. By taking the difference among the timing of two consecutive spikes, samples of the inter-spike interval (ISI) can be calculated. The ISI is related to the First Passage Time (FPT) problem as described next.

Consider the Ito stochastic differential equation of the form (Equation 2.1) governing the process X_t. Let y_0 be a deterministic constant. The FPT is a random variable T defined as the

time t after time t_0, at which X_t first hits y_0 starting from some initial value X_{t_0} smaller than y_0. Formally, T is defined as:

$$T = \inf\{t \geq t_0 : \ X_t \geq y_0, X_{t_0} < y_0\}. \tag{2.7}$$

The FPT distribution function is thus:

$$f_T(t; x_0, y_0) = \frac{\partial}{\partial t} P[T \leq t], \tag{2.8}$$

where T is defined in (Equation 2.7) and $X_{t_0} = x_0$. Although a closed form expression for $f_T(t; x_0, y_0)$ is not available, its moments can be numerically approximated by using the Laplace transform, g_λ of $f_T(t; x_0, y_0)$ with respect to t (64) as

$$m_n(x_0, y_0) \triangleq E[T^n | X_{t_0} = x_0 < y_0] = (-1)^n \frac{d^n g_\lambda}{d\lambda^n}|_{\lambda=0}, \tag{2.9}$$

where g_λ satisfies (65) :

$$\frac{\sigma^2}{2}\frac{d^2 g_\lambda}{dx_0^2} + (\frac{x_0}{\theta} - \mu)\frac{dg_\lambda}{dx_0} - \lambda g_\lambda = 0 \tag{2.10}$$

$$\lim_{x_0 \to S} g_\lambda = 1$$

$$\lim_{x_0 \to -\infty} g_\lambda = 0$$

It is well known that a neuron releases a spike whenever its membrane potential X_t exceeds a threshold y_0 which is assumed to be constant over time. After spiking, the membrane potential is reset to $x_0 < y_0$. The FPT in the context of neuronal activity is thus the time in between two consecutive spikes, that is, T is the inter spike interval (ISI). The density of the FPT, or of the ISI, thus depends on five parameters: μ, σ, θ, y_0 and x_0. The first two parameters (the drift μ and the diffusion σ) are the input parameters and are related to the neuronal membrane potential dynamics that are to be extracted from recorded data. The last three parameters (the membrane time constant θ, the firing threshold y_0 and the membrane resting potential x_0) are intrinsic parameters of the neuron and are set to biologically plausible values. Since the mean (i.e., $n = 1$ in Equation 2.9) and power (i.e., $n = 2$ in Equation 2.9) of the ISI distribution is all that is needed to extract the drift and diffusion coefficients, the problem of parameter identification for the OUP reduces to that of computing the sample mean and sample power from the recorded data and then solving the corresponding two equations from Equation 2.9 for μ and σ as will be discussed in Section 2.3. Thus, the complexity of extracting μ and σ in Equation 2.1 boils down to a sample mean and sample variance estimation from the measured ISI samples.

2.3 Methods

2.3.1 Data Set

For the numerical results presented in this section, data was collected during routine recording of neuronal activity in PD and ET patients undergoing surgery for DBS as a part of surgical mapping during DBS electrode implantation. This recording is done by the surgeon to pre-

cisely locate the target of DBS electrode insertion by assessing the neuronal spike form as well as the neuronal firing rate at different depths from the target (66). An IRB approval (2008-0176, UIC) was obtained for accessing the data recorded and stored during surgery for DBS implantation on PD patients. The recording was performed with a MicroTARGETING micro-electrode manufactured by FHC, Inc. (Bowdoinham,ME) and processed/ recorded using NeuroTrek micro-recording device manufactured by AlphaOmega Engineering (Alpharetta, GA). The data was sampled at 25.21 KHz and was high pass filtered at 200Hz to cut off low frequency noise.

A single recording consists of neuronal activity in the form of potential difference across the membrane of a neuron. Since the recording is *extra-cellular*, there is some background activity superimposed with the spikes generated by a single neuron. It is practically impossible to separate *in vivo* the activity of a single neuron from the background activity. The background activity is typically generated by neighboring neuronal activity and some measurement noise. The timestamps of spike occurrences in the recorded data are determined by the surgeon at the time of recording by adjusting a threshold. The software automatically records the time instants when the voltage crosses the set threshold to yield these timestamps. This determines the firing frequency (average number of action potential pulses per second). The high-pass filtering eliminates all action potentials with a duration greater than 5 ms (corresponding to 200 Hz) (67).

The ISI required for the parameter extraction from the recorded spike timings is calculated as the difference between the consecutive spike timings. The empirical ISI probability distribu-

tion is then estimated from the calculated ISI using a bin width determined by the Freedman Diaconis rule (68) according to which:

$$h = 2\frac{IQR(x)}{n^{1/3}}, \tag{2.11}$$

where h is the bin width, IQR is the inter-quartile range of the data x and n is the number of data samples. This distribution is referred to in the rest of the section as the measured ISI distribution.

2.3.2 OUP Parameter Extraction

The parameters of the model in Equation 2.1 μ (the drift coefficient) and σ (the diffusion coefficient) can be considered constant over the recording interval (in the order of seconds or minutes) for a data set at a particular target. Hence, the mean and standard deviation (std) of the ISIs are calculated over the entire data segment for parameter extraction. This is further verified by calculating the mean and std over non-overlapping windows of around 1 s. μ and σ are estimated for different values of θ (the membrane time constant) and fixed values of x_0 and y_0 by following the method proposed in (69) which is described briefly in the following paragraph.

The OUP as in Equation 2.1 involving five parameters, $\mu, \sigma, x_0, y_0, \theta$ is first normalized to reduce the number of parameters. The following transformation is used:

$$X' = \sqrt{2/\sigma^2\theta}(x - \mu\theta), t' = t/\theta \tag{2.12}$$

which transforms Equation 2.1 to the normalized OUP which satisfies:

$$dX'(t') = -X'(t')dt' + \sqrt{2}dW(t') \tag{2.13}$$

$$\xi = \sqrt{2/\sigma^2\theta}(x_0 - \mu\theta)$$

$$\eta = \sqrt{2/\sigma^2\theta}(y_0 - \mu\theta), -\infty < \xi < \eta < \infty$$

where ξ is the new initial state and η is the new threshold. The OUP-FPT distribution, $g'(\eta, t'/\xi)$ and the n-th moment, $M_n(\xi, \eta)$ of the normalized OUP is related to those of the OUP according to:

$$g(y_0, t/x_0) = g'(\eta, t'/\xi)/\theta \tag{2.14}$$

$$m_n(x_0, y_0) = \theta^n M_n(\xi, \eta)$$

The first two moments of the OUP-FPT can be evaluated as (64):

$$M_1(\xi, \eta) = \phi_1(\eta) - \phi_1(\xi) \tag{2.15}$$

$$M_2(\xi, \eta) = 2\phi_1^2(\eta) - \phi_2(\eta) - 2\phi_1(\eta)\phi_1(\xi) + \phi_2(\xi), \eta \geq \xi$$

where,

$$\phi_1(z) = \frac{k}{2}\sum_{n=1}^{\infty}\frac{(\sqrt{2}z)^n}{n!}\Gamma(n/2) \tag{2.16}$$
$$\phi_2(z) = \frac{k}{4}\sum_{n=1}^{\infty}\frac{(\sqrt{2}z)^n}{n!}\Gamma(n/2)(\psi(n/2) - \psi(1))$$

$\Gamma(z) = \int_0^\infty t^{z-1}e^{-t}dt$ and

$\psi(z) = \Gamma'(z)/\Gamma(z)$ being the gamma and the digamma functions respectively.

Let m_1 and m_2 be the first and the second moments of the measured ISIs which are equated to the first two moments of the OUP-FPT distribution as in Equation 2.14 and Equation 2.15:

$$\theta M_1(\xi, \eta) = m_1 \tag{2.17}$$
$$\theta^2 M_2(\xi, \eta) = m_2$$

Equation 2.17 is then solved (using the fsolve function in MATLAB which finds a root of a set of nonlinear equations) for fixed values of $x_0 = 0$ (the resting membrane potential), $y_0 = 15$mV (the firing threshold), and θ (the membrane time constant) ranging from 1ms to 25ms in steps of 0.2ms to determine ξ and η. The physiological value of θ can be $1 - 20$ms (70) and can serve as a guide to choose θ. However, it is a free parameter in the model and uniquely determines μ and σ from ξ and η (Equation 2.13) to match the first two moments as calculated from the measured samples.

2.3.3 Evaluating performance of the Proposed Approach

The OUP parameters are identified by simply matching the first two moments and hence are not optimized according to any criterion. In order to choose the best set of values for (θ, μ, σ) that would produce the same set of mean and variance as that measured from the samples, we proceed as follows. Once the parameter values are extracted, the ISI distribution is simulated by numerically solving an integral equation as in (71) with $x_0 = 0$, $y_0 = 15$mV, and θ ranging from 1ms to 50ms in steps of 0.2ms. This numerically simulated ISI distribution is referred to in the rest of the work as the simulated ISI distribution. Without any prior knowledge about the underlying distribution that governs the real ISI distribution, two types of distance measures were considered:

1) An integral squared error (ISE) of distribution as a metric to compare the simulated ISI distribution with the measured one. This quantifies the goodness of fit instead of just a graphical illustration as in (69). The ISE is obtained by calculating the sum of the squared error between the values of the measured and simulated ISI distribution at each bin. At each bin, the value of the simulated probability distribution is calculated as the value of the simulated probability density at the bin center times the bin width. A better fit would correspond to a lower value of ISE.

2) KullbackLeibler (KL) divergence (72) is a non-symmetric measure of the difference between

two probability distributions. For probability distributions P and Q of a discrete random variable, their KL divergence is defined as:

$$D_{KL}(P||Q) = \sum_i P(i) log \frac{P(i)}{Q(i)}. \tag{2.18}$$

where Q is the simulated distribution, P is the measured isi distribution and the summation is over the bins which have non-zero distribution values. Lower the value of D_{KL}, better the fit is.

3) A cumulative distribution function (CDF) from the simulated ISIs following (Equation 2.1) was calculated and compared with the one estimated from the recorded data. A Kolmogorov-Smirnoff (KS) test (73) was performed between the measured ISI samples and the simulated CDF of the OUP-FPT distribution. This tests the null-hypothesis that the recorded data are from the simulated distribution against the hypothesis that the samples are not from the simulated distribution. A higher p-value indicates a greater probability of recorded ISI samples having the same underlying distribution as the simulated one. Hence the p-value is an indicative of the goodness of fit.

2.3.4 Comparison with other approaches

To compare the OUP model with existing stochastic models, the measured ISI distribution was fitted to the exponential distribution arising from a Poisson Process (PP) and to an inverse Gaussian (IG) distribution arising from a random walk model (52). The PP model of neuronal

membrane potential would generate ISIs distributed according to the exponential distribution which is defined as:

$$f_{PP}(x;\mu^*_{ex}) = \frac{1}{\mu^*_{ex}} \mathrm{e}^{-\frac{x}{\mu^*_{ex}}} 1_{[x\geq 0]} \tag{2.19}$$

where μ^*_{ex} in (Equation 2.19) is the mean of the distribution. μ^*_{ex} can be estimated from the sample ISIs as the maximum likelihood (ML) estimate (maximizing the log likelihood function) or by minimizing the ISE criterion as described in section 2.3.3. The ML estimate of μ^{ml}_{ex} is the sample mean ISI (not to be confused with the mean of the OUP process X_t, which is indicated with the symbol μ). μ^*_{ex} was also estimated by minimizing the ISE and is denoted as μ^{mise}_{ex} and referred to as the MISE parameter estimate. This is done by using the lsqcurvefit function in MATLAB and using the ML estimate as the initial value.

The random walk model for the neuronal membrane potential, which is essentially a (Gaussian) Wiener Process (WP) has the following Langevin equation:

$$dX(t) = \mu_{wp}dt + \sigma_{wp}dW(t), \tag{2.20}$$

where $dW(t)$ is a zero-mean white Gaussian process with variance dt. The FPT distribution of the is an IG distribution (52) given by:

$$f_{IG}(x;\mu^*_{ig},\lambda) = \sqrt{\frac{\lambda}{2\pi x^3}} \exp\left\{\frac{-\lambda(x-\mu^*_{ig})^2}{2(\mu^*_{ig})^2 x}\right\} 1_{[x\geq 0]}, \tag{2.21}$$

where μ_{ig}^* is the mean and $(\mu_{ig}^*)^3/\lambda$ is the variance of the IG distribution . The IG parameters are related to the parameters of the generated WP as: $\mu_{wp} = y_0/\mu_{ig}^*$, $\sigma_{wp} = y_0/\sqrt{\lambda_{ig}^*}$, y_0 is the threshold. The maximum likelihood estimation method proposed in (74) is used for estimating the model parameters μ_{ig}^* and λ as μ_{ig}^{ml} and λ^{ml}, respectively. Using a similar technique as for the exponential distribution parameter (minimizing the ISE), μ_{ig}^{mise} and λ^{mise} are also estimated and are referred to as the MISE parameter estimates.

The performance analysis as discussed in Section 2.3.3 was also performed for the simulated exponential and IG distributions with respect to the measured ISI distribution.

2.4 Results and Discussion

2.4.1 PD data

The neuronal data used for modeling was recorded from the left and right STN of a PD patient undergoing surgery for DBS. The recorded segments selected for analysis by the neurosurgeon was based on the purity of signal recorded in the operating room, uniformity of recorded discharges, and a typical discharge pattern (in terms of discharge amplitude, frequency and presence of irregular bursts) corresponding to expected activity in parkinsonian STN (66). The average firing rate was 56 and 54 spikes/s on the left and the right STN respectively.

An enlarged portion of the recorded segments are shown in Figure 1. The calculated ISI from the recorded data were then used to obtain the empirical ISI probability distribution using bin width determined according to the Freedman Diaconis rule.

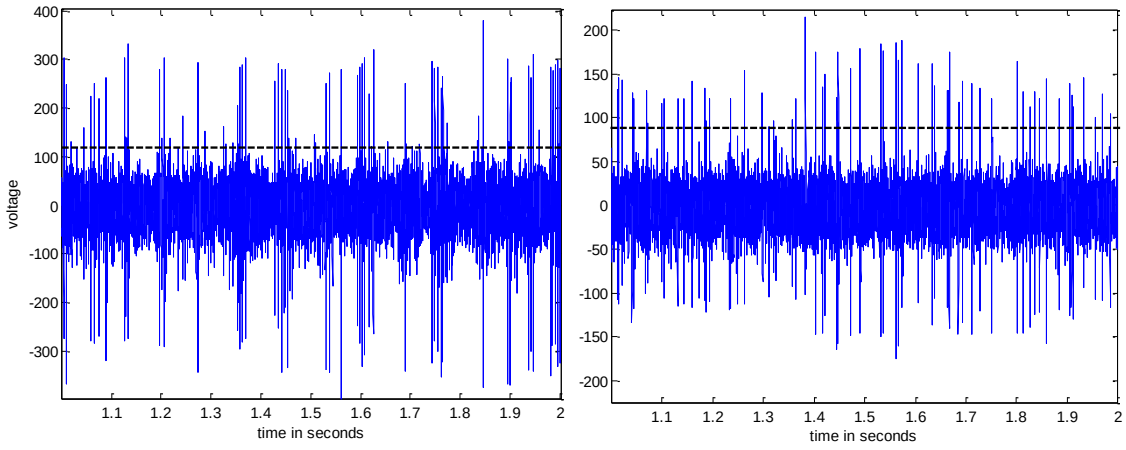

Figure 1. An enlarged portion of the recorded signal on the (left) left STN and (right) right STN. The dashed line is the threshold set by the surgeon to determine the spikes.

Left STN data

The sample mean and sample standard deviation of the measured ISIs on the left STN over the entire data segment of 11s, were found to be 17.8ms (i.e., the firing rate is 56 spikes/second) and 22.7ms, respectively. Further, the data was divided into 3 non-overlapping windows of 4, 4 and 3 seconds duration, and the sample mean and standard deviation were calculated over these 3 windows as shown in Figure 2 (top left). As seen from Figure 2, the mean and the standard deviation have very similar values over the three windows, thus the assumption of data stationarity (at least up to the second moment) over the recording interval is valid.

Figure 2 (top left) and Figure 2 (bottom left) show μ in mV/s and σ in mV/$\sqrt{\text{s}}$, respectively, plotted against the membrane time constant θ in millisecond for the left STN dataset. Thus, for each value of θ, the value of μ and σ as in Figure 2 constitute a set of μ, σ, θ that would generate an ISI distribution with the same mean and std as the those of the measured ISI. The calculated ISE corresponding to θ values from 5ms to 25ms are plotted in Figure 2 (bottom left). From Figure 2, it can be seen that any value of θ between $14-25$ ms will produce an ISE in the

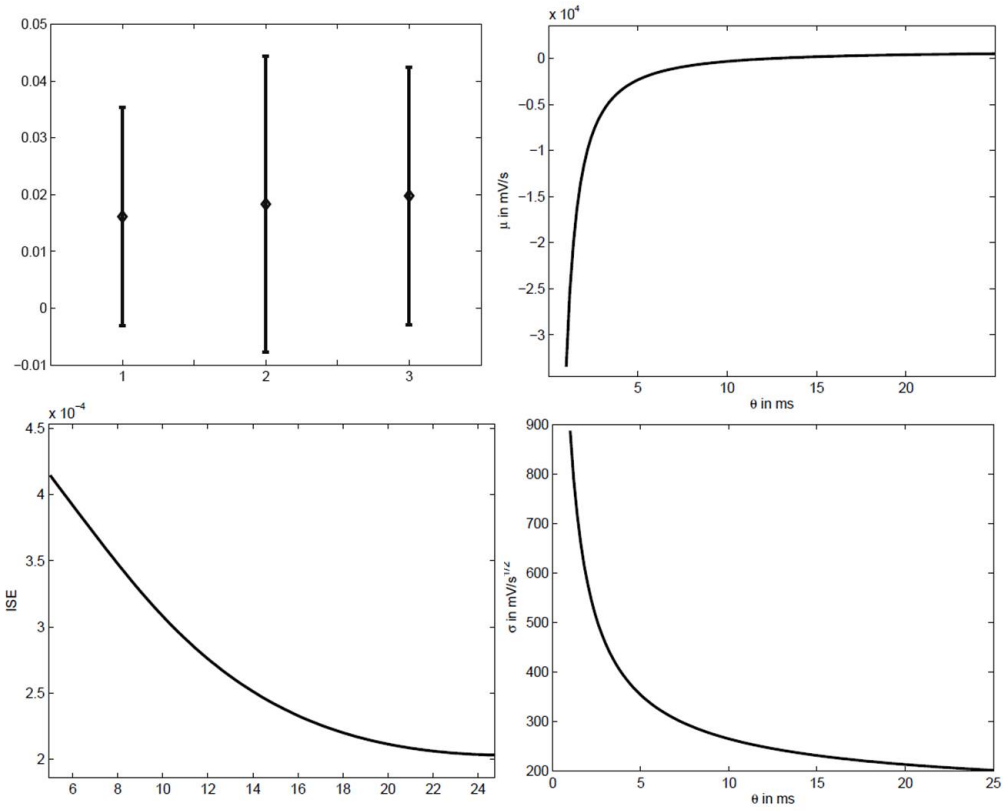

Figure 2. left: (top)The mean and standard deviation of measured ISIs over 3 non-overlapping data windows of 4,4 and 3 seconds, (bottom)ISE between measured and simulated ISI distribution plotted against the membrane time constant θ in ms; right: (top)Model parameter μ in mV/s, (bottom)σ in mV/$\sqrt{\text{s}}$ plotted against the membrane time constant θ in ms. All the data corresponds to left STN.

range $(0.202 - 0.250) \times 10^{-3}$. Figure 3 shows the ISI distribution calculated from measured left STN data (solid line) along with the simulated ISI distribution (in dashed line) corresponding to $\theta = 15ms$ and $\theta = 20ms$. The x-axis shows the time in seconds while the y-axis shows the probability distribution function. We observe that a low ISE value (an objective performance measure) indeed corresponds to a good "visual fit".

Figure 4 shows the ISI CDF calculated from measured left STN data (dashed line) along with the simulated ISI distribution (in solid line) corresponding to $\theta = 15ms$ and $\theta = 20ms$. The x-axis shows the time in seconds while the y-axis shows the cumulative probability distribution function (CDF).

For the exponential distribution in (Equation 2.19), the parameters identified were: $\mu_{ex}^{ml} = 0.0178$s and $\mu_{ex}^{mise} = 0.0100$s. The IG distribution (Equation 2.21) parameters μ_{ig}^{*} and λ were estimated to be $\mu_{ig}^{ml} = 0.0178$s, $\lambda^{ml} = 0.0068$s, $\mu_{ig}^{mise} = 0.0349$s and $\lambda^{mise} = 0.0075$s. All the model parameters are included in Table II. The exponential and the IG probability distribution were simulated using both the respective ML and MISE parameter estimates and the ISE between the measured and the simulated distributions are tabulated in Table I.

The OUP-FPT distribution clearly performs better than the exponential and the IG (corresponding to the ML parameter estimates) distributions in terms of the ISE and D_{KL} values. However, the OUP-FPT and the IG (corresponding to the MISE parameter estimates) distributions have comparable performance.

Both OUP and WP (corresponding to the IG distribution) with corresponding estimated parameters were used to simulate the membrane potential to verify the firing pattern. The

TABLE I

ISE VALUES FOR THE OUP-FPT, EXPONENTIAL AND IG DISTRIBUTIONS.

Distributions	ISE values	D_{KL}
OUP-FPT($\theta = 14 - 25ms$)	$(\mathbf{0.20 - 0.25}) \times 10^{-3}$	$\mathbf{0.0313 - 0.0317}$
exponential(ML)	0.93×10^{-3}	0.1344
exponential(MISE)	0.37×10^{-3}	0.1636
IG(ML)	0.22×10^{-3}	0.0622
IG(MISE)	0.20×10^{-3}	0.0679

TABLE II

MODEL PARAMETERS FOR LEFT STN DATA.

OUP-FPT			
θ in ms	μ in mV/s	σ in mV/$\sqrt{s}$	
20	389.53	213.32	
Inverse Gaussian			
μ_{ig}^{ml}	λ^{ml}	μ_{ig}^{mise}	λ_{ig}^{mise}
0.0178 s	0.0068 s	0.0349 s	0.0075
Exponential			
μ_{ex}^{ml}		μ_{ex}^{mise}	
0.0178 s		0.01 s	

membrane potential was simulated by using Equation 2.1 with sampling time set to 0.04ms. At each time point, the voltage X_t of the membrane was calculated using Equation 2.1. At the times the voltage exceeds the threshold value $y_0 = 15$ mV a randomly selected action potential waveform from a dictionary of five types of action potential waveform extracted from the measured data was put at that time instant, and X_t was reset to the resting potential $x_0 = 0$. The value of X_t thus simulated is the sub-threshold activity, i.e, the membrane potential that does not cross the threshold of 15 mV, of a single neuron in isolation. As remarked in Section 2.3.1, it is not possible to record *in vivo* the time evolution of the membrane potential of single neuron in isolation, since the measurements also include a "background noise" given by the aggregate activity of the surrounding neurons.

Figure 6 shows a part of the simulated signal (top left) as well as the average firing rate (number of spikes/second) (bottom left) calculated over the entire duration of 11s. The MISE parameter estimates corresponding to the IG distribution (which produced similar ISE values as the OUP-FPT) were also used to simulate the membrane potential which evolves in time following the corresponding WP in Equation 2.20. Figure 6 shows a part of the simulated signal following the WP (top right) as well as the average firing rate (number of spikes/second) calculated over the entire duration of 11s. The n-th point ($n = 1, 2, ..., 11$) in Figure 6 (bottom) corresponds to the number of spikes during $(n-1)$-th to n-th second interval in the signal.

The OUP produces an average firing rate of (52 ± 10.4) spikes/s while the WP produces an average firing rate of (25.7 ± 8) spikes/s, the measured average firing rate being (56 ± 9.45) spikes/s. This is because the MISE parameters are estimated such that the mean-squared error

between the measured and the IG distribution is minimized, and hence does not take into account the first and second moments of the measured ISI samples. These parameters will also be highly dependent on the bin selection.

Right STN data

The neuronal data recorded from the right STN was used to calculate ISI samples which were in turn used to identify the OUP parameters, θ, μ, σ, the IG parameters, $\mu_{ig}^{ml}, \lambda_{ig}^{ml}$ as well as the exponential parameter, μ_{ex}^{ml}. The MISE parameters corresponding to the IG and exponential model were not calculated for this data set because as was seen for the left STN data set, these parameters do not conserve the mean of the measured ISI samples. Additionally, a KS test was performed to test if the recorded ISI samples are drawn from the fitted OUP-FPT, IG or exponential distribution which produced a p-value.

Table VI shows the different model parameters while Table V shows the ISE, D_{KL} and p-value for the three fitted distributions. For each case, the distribution that has the best performance is marked in bold. It can be seen that the OUP-FPT performs the best for all the cases.

Since the OUP FPT distribution closely follows the empirical ISI distribution as well as the OUP generates similar firing rates as the measured one, the OUP (Equation 2.4) can be used to model the neuronal activity of the STN in PD patients. The parameters are however expected to vary for different recording targets in the same patient, for different patients and might as well vary over long time intervals (with progression of disease) for the same location in a particular patient.

TABLE III

ISE, D_{KL} AND P-VALUES (FROM K-S TEST) FOR THE OUP-FPT, EXPONENTIAL AND IG DISTRIBUTIONS FITTED TO THE RIGHT STN DATA.

Distributions	ISE values	D_{KL}	p-value
OUP-FPT($\theta = 6.5ms$)	$\mathbf{0.28 \times 10^{-3}}$	**0.0736**	**0.05**
exponential(ML)	0.4×10^{-3}	0.0789	2×10^{-7}
IG(ML)	0.42×10^{-3}	0.0821	1.8×10^{-8}

TABLE IV

MODEL PARAMETERS FOR RIGHT STN DATA.

OUP-FPT		
θ in ms	μ in mV/s	σ in mV/$\sqrt{s}$
6.5	1485.4	110.4
Inverse Gaussian		
μ_{ig}^{ml}	λ^{ml}	
0.0184 s	0.0157 s	
Exponential		
μ_{ex}^{ml}		
0.0184 s		

2.4.2 ET data

This recording was performed during surgical implantation of DBS electrode into the VIM of thalamus of an adult (awake) ET patient at the UIC Medical Center as an IRB-approved research project. The surgery was performed on both sides of the patient's brain in one session. Recording of neuronal electrical activity was performed before, during and immediately after applying test electrical stimulation to the VIM in thalamus. Standard microrecording electrodes (Alpha-Omega Engineering, Nazareth Illit, Israel) was used, that allow delivering stimulation

through the tip of the microelectrode (microstimulation) or through the integrated guiding cannula ring (macrostimulation) located 3 mm above the microelectrode tip (67). The procedure of stimulation/recording was performed on both sides, first on the left, and then on the right side. During the surgical mapping process, two identical microelectrodes were inserted at a distance of 2mm from each other (referred as Electrodes 1 and 2). Both of them were used for simultaneous recording while the macrostimulation was delivered from Electrode 1, with effective distance between recording and stimulation sites of 3mm and 3.6mm for Electrodes 1 and 2, respectively.

Theoretically, a macroelectrode records the low frequency local field potential while a microelectrode records the high frequency firing activity from a single neuron. However, when either of them is used for stimulating, the same contact cannot record; the recording from the other contact of same electrode is saturated due to the high stimulus voltage. Hence, when stimulating, the other neighboring electrode is used for recording. In this case, the microelectrodes served to continuously record the neuronal activity of the thalamus before, during and after stimulation. The recording was made using NeuroNav device (Alpha-Omega Engineering), at a sampling rate of 24kHz. Stimulation was applied at two pulse rates, namely, at 130Hz and at 160Hz and with a pulse width of 60 microseconds. Pulse trains of durations of 15, 30 and 40sec were applied at varying intervals between trains on both the left and right VIM of thalamus.

In the absence of an external stimulus, the timestamps of spike occurrences were detected by setting a threshold that was determined by the neurosurgeon by visual inspection of the recorded data. When a train of high frequency pulses was applied, spikes could be extracted

from the voltage recorded by the electrode adjacent to the stimulating electrode. The recording still had stimulation artifacts. By subtracting the stimulation artifacts, the spikes in between stimulus pulses could be recovered. In the latter case, only the time interval when there was no stimulus artifact was considered since it is not possible to determine if there were spikes embedded in the artifacts. The ISI required for parameter extraction were obtained from the detected spike timings as the difference between consecutive spike times.

Analysis of the following recorded data are presented: (a) before, during and after 30s train of stimulus on the left side, and (b) before, during and after 40s train of stimulus on the right side. In both cases the stimulation was at 160Hz and was applied through the outer macroelectrode 1 while the data was recorded by microelectrode 2. Portions of the recorded data before, during and after stimulation are shown in Figure 8.

For each set of data, ISIs were calculated from the spike times and the CDF was estimated (with the Matlab function `ecdf`). The probability distribution was estimated by binning the sample ISIs with bin size determined according to Equation 2.11. The OUP parameters μ, σ as described in Section 2.3.2 were estimated for a wide range of θ depending on whether the recorded signal is with or without stimulus. The set of parameters that produced the best fit are tabulated in Table V together with the mean and standard deviation of the recorded data. The parameters of the IG (μ_{ig}^{ml}, λ^{ml}) and of the exponential (μ_{ex}^{ml}) distribution were ML estimated as in (74). The $\mu_{ig}^{mise}, \lambda^{mise}, \mu_{ex}^{mise}$ were not considered for this data set because, although it produces a good fit to the empirical distribution, it is highly dependent on the bin size as well as it changes the mean and std of the simulated distribution as was seen in the PD dataset.

TABLE V

OUP PARAMETERS FOR ET DATA SET.

Data type	μ_{ou} [mV/s]	σ [mVs$^{-1/2}$]	θ [sec]	mean±std
Left VIM				
Before stim.	656.33	82.92	0.0167	0.0336±0.0272
During stim.	201.77	92.54	0.1218	0.0609±0.0726
After stim.	860.64	62.13	0.0241	0.0241±0.015
Right VIM				
Before stim.	754.69	125.47	0.0085	0.0256±0.0228
During stim.	2.57	65.98	0.2720	0.2720±0.3718
After stim.	360.59	63.90	0.0500	0.0498±0.0415

In order to establish which distribution best fit the recorded data, a KS test was performed between the measured ISI samples and the simulated CDF of the three distributions. The p-values obtained from the test corresponding to each distribution are tabulated in Table VI. A higher p-value indicates a greater probability of the simulated samples and the recorded data having the same underlying distribution. Hence the p-value is an indicative of the goodness of fit. Additionally, the ISE and D_{KL} values were calculated for each distribution, a lower value of ISE and D_{KL} corresponding to better fit. Figure 9 and Figure 10 show the simulated CDF for the three distributions fitted to ISIs measured from the right and the left VIM respectively. Table VI shows that the OUP-FPT has either comparable or much higher p-values than the other two distributions for ISI samples measured from both sides and under all conditions. The exponential performs relatively better for samples during stimulus while the IG has a good performance for samples without stimulus on the left side. The IG however has very poor

TABLE VI

P-VALUES FROM THE KS TEST FOR DIFFERENT DISTRIBUTIONS.

Data type	Exponential	IG	OUP-FPT
Left VIM			
Before stim.	0.42×10^{-16}	0.20	**0.23**
During stim.	**0.05**	0.53×10^{-41}	0.04
After stim.	0.57×10^{-15}	0.746	**0.835**
Right VIM			
Before stim.	0.034	6.87×10^{-7}	**0.568**
During stim.	0.087	0.373×10^{-41}	**0.130**
After stim.	0.112×10^{-15}	0.73×10^{-45}	**0.170**

TABLE VII

ISE AND D_{KL} VALUES FOR DIFFERENT DISTRIBUTIONS.

Data type	ISE ($\times10^{-4}$)			D_{KL}		
	OUP-FPT	IG	exponential	OUP-FPT	IG	exponential
Left VIM						
Before stim.	**0.52**	0.97	0.81	**0.030**	0.049	0.132
During stim.	8.14	48.0	**3.06**	0.353	0.840	**0.187**
After stim.	**0.97**	1.18	21	0.063	**0.062**	0.302
Right VIM						
Before stim.	**2.37**	4.02	3.48	**0.045**	0.056	0.051
During stim.	7.64	36.0	**4.56**	**0.114**	0.238	0.124
After stim.	**0.89**	40.0	10.0	**0.047**	0.445	0.177

performance for the right side with very low p-values. Table VII shows a similar trend with the ISE and D_{KL} values. In Table VI and Table VII, the winners in each category are in bold which shows that the OUP-FPT has the best performance in maximum number of cases. The better performance of the OUP can be explained as follows: the free parameter θ has the power of tuning the OUP parameters to obtain a good fit. θ also offers a good indication of the presence and absence of stimulus, or the transition from ON to OFF stimulation states (notice the wide difference in the values of θ for data with and without stimulus in Table V). The exponential and the IG have comparable performances for selected cases but in general cannot produce good fits for all ranges of the recorded data. Figure 9 and Figure 10 corroborate these facts and we can see a direct correlation between a high p-value and a good visual fit.

Neurological data is highly stochastic in nature. Stochastic models of neuronal activity are thus a natural choice, and they are much more robust and require lesser parameters than their deterministic counterparts. The Fokker-Planck equation provides an efficient method of formulating a deterministic evolution equation that governs the dynamics of the probability density function. The major drawback of this approach is that analytical solutions to the Fokker-Planck equation are seldom found. Hence, efficient numerical algorithms must be devised to solve the (generally tough) reverse problem of the model parameter extraction.
The OUP (57) is fairly simple and yet captures the main physiological characteristic of the neuronal firing process.

The model parameter identification can be done quickly and efficiently following the method by (69) from the sample mean and sample variance of the measured ISI. This method is however

not optimized according to any criterion and is simply matching of the first two moments. Hence, with an accurate model of the neuronal activity of PD and ET patients and with an efficient and fast algorithm to identify its parameters, the OUP model can be used to predict the effects of DBS stimulation. This will enable the design of time-adaptive DBS stimulation that can be tailored to the needs of each individual patient. However, to reach this goal, the model must be modified to include a forcing function mimicking the effect of an external input such as a train of high frequency pulses as is used in DBS to test its effect on the firing activity. Alternatively, the model parameters can be altered to account for stimulation.

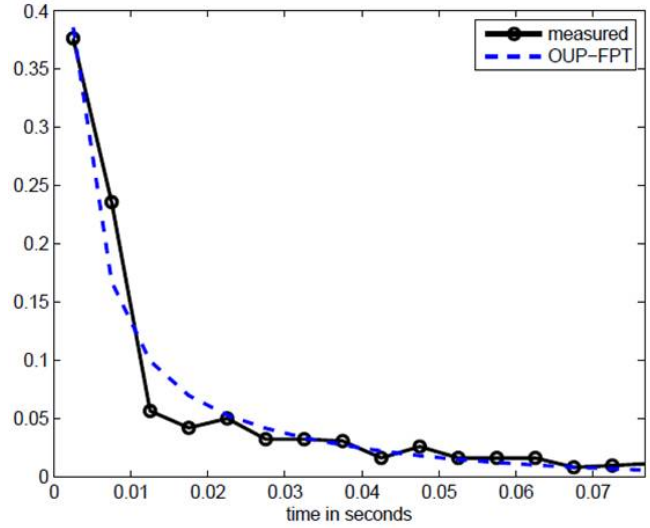

(a) $\theta = 15ms$.

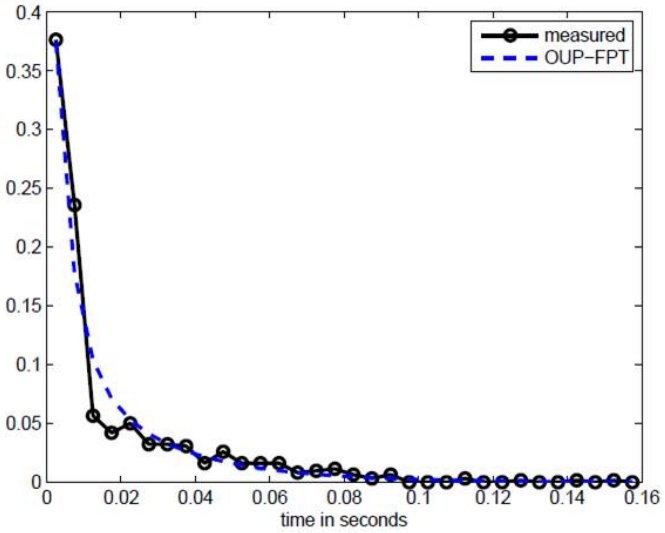

(b) $\theta = 20ms$.

Figure 3. ISI probability distribution of the measured PD data (in solid line) and of the simulated OUP (in dashed line), (a) for θ =15ms. (b) for θ =20ms.

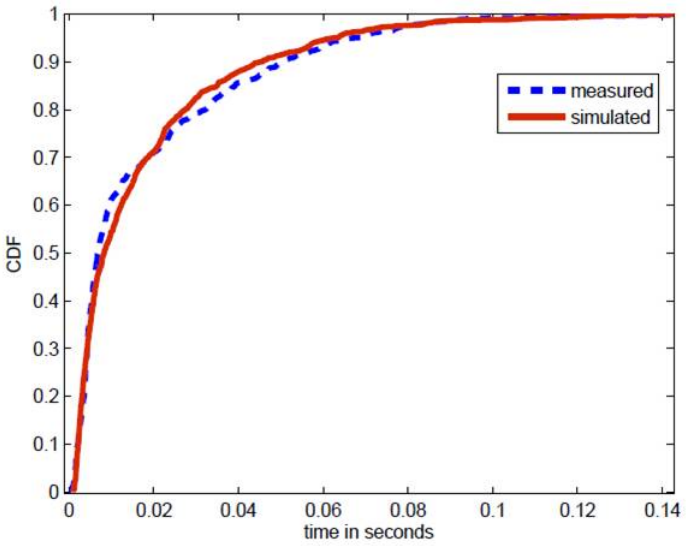

(a) $\theta = 15ms$.

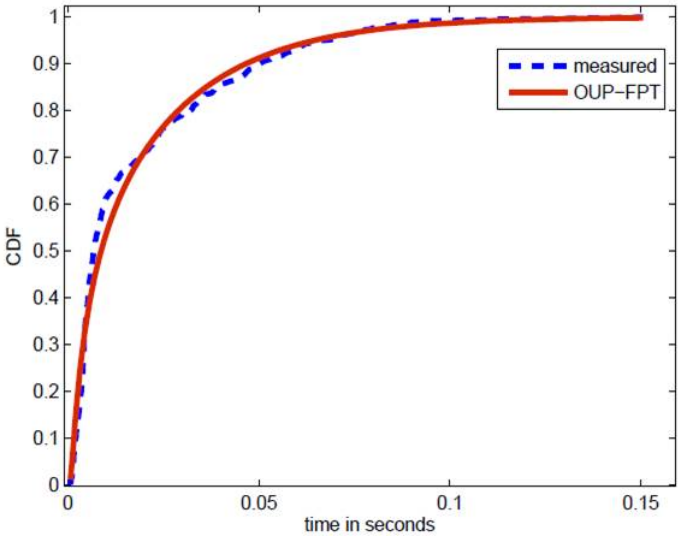

(b) $\theta = 20ms$.

Figure 4. ISI cumulative distribution of the measured PD data (in dashed line) and of the simulated OUP (in solid line), (a) for θ =15ms. (b) for θ =20ms.

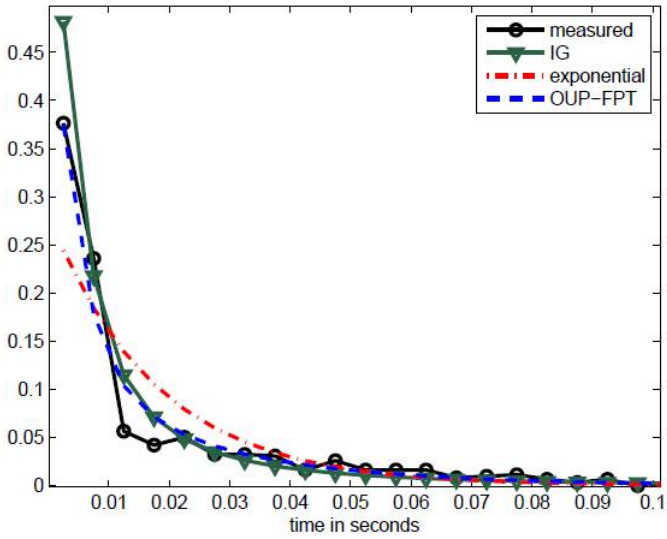

(a) Simulated distributions for ML parameter estimates.

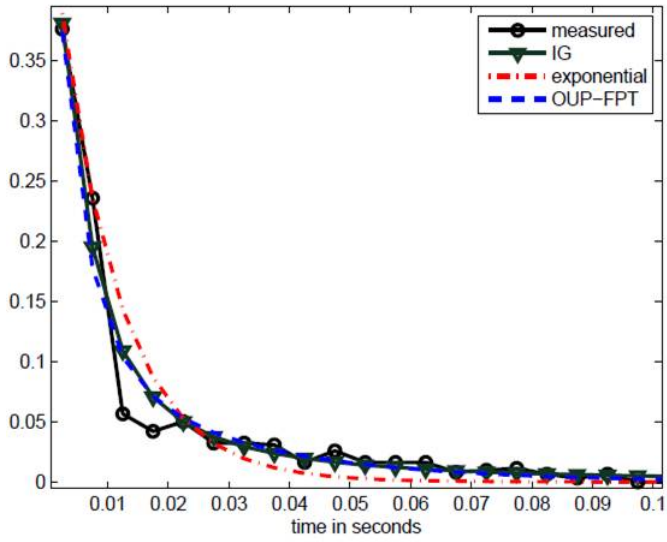

(b) Simulated distributions for MISE parameter estimates.

Figure 5. A comparison between IG (line with triangular markers),exponential (dash-dot line) and OUP-FPT(dashed line) distributions fitted to ISI distribution of recorded data (line with circle markers) from PD patient. (a) corresponding to $\theta = 20ms$ for OUP-FPT and ML parameter estimates of the exponential and IG distribution. (b) corresponding to $\theta = 20ms$ for OUP-FPT and MISE parameter estimates of the exponential and IG distribution.

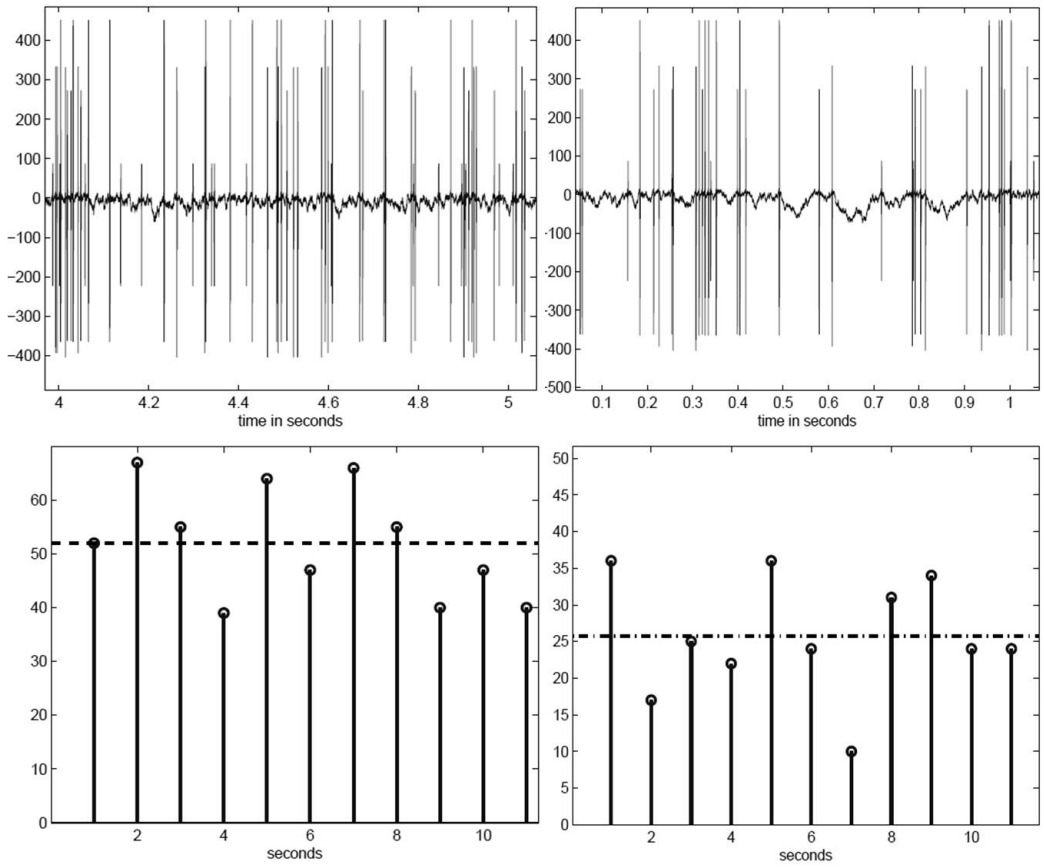

Figure 6. top: part of the simulated membrane potential according to (left)OUP (Equation 2.1), (right)WP (Equation 2.20) for PD patient; bottom: The number of spikes/second over a duration of 11 s for (left)OUP, (right)WP. The dotted line indicates the average firing rate over the entire interval.

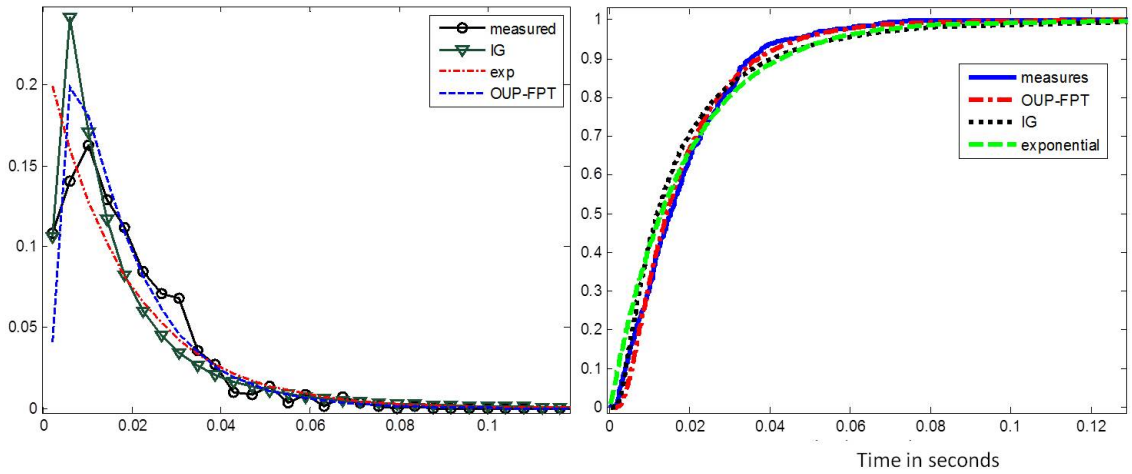

Figure 7. Comparison of different distributions fitted to ISI samples measured from the right STN. (left) Probability distribution, (right) Cummulative distribution function.

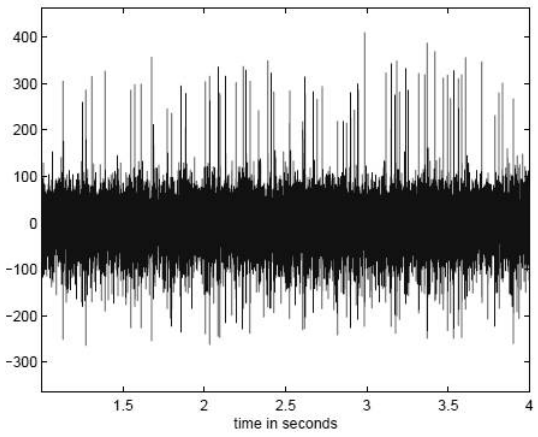

(a) Signal before stimulation.

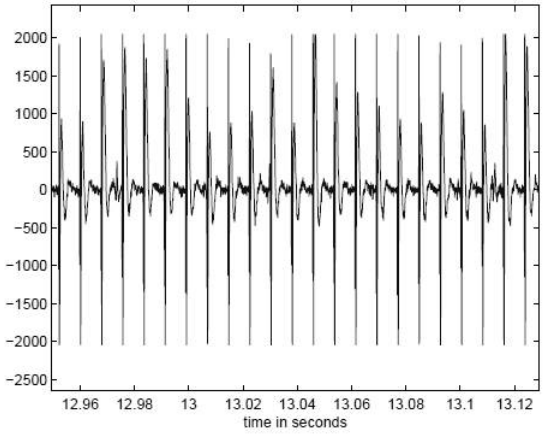

(b) Signal during stimulation.

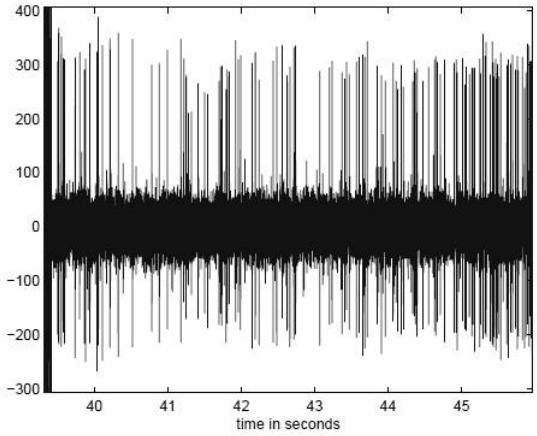

(c) Signal after stimulation.

Figure 8. A portion of the signal measured from the right VIM of ET patient. (a) Before applying any stimulus. (b) During a train of 160 Hz pulses for 40s. (c) Immediately after the stimulus.

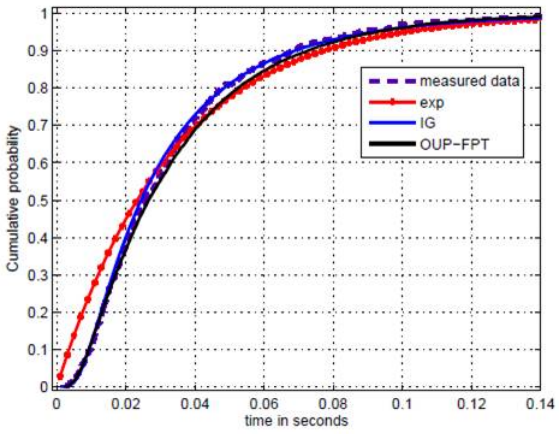

(a) Before stimulation.

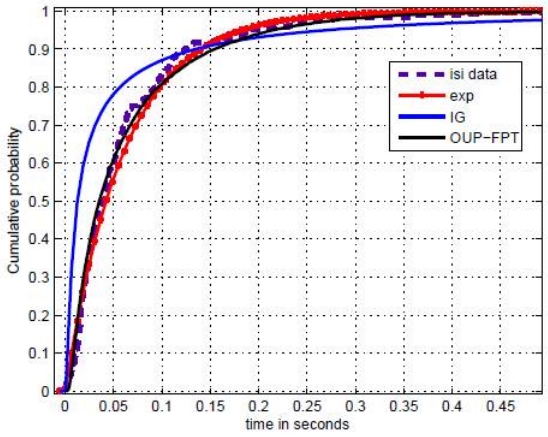

(b) During stimulation.

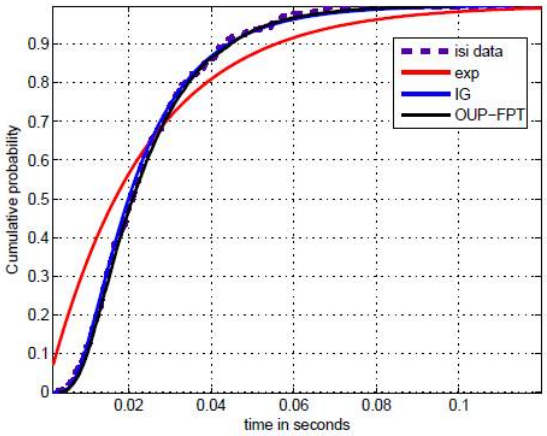

(c) After stimulation.

Figure 9. Comparison between IG, exponential and OUP-FPT CDFs fitted to the measured ISIs from the left VIM of ET patient. (a) Before applying any stimulus. (b) During a train of 160 Hz pulses for 30s. (c) Immediately after the stimulus.

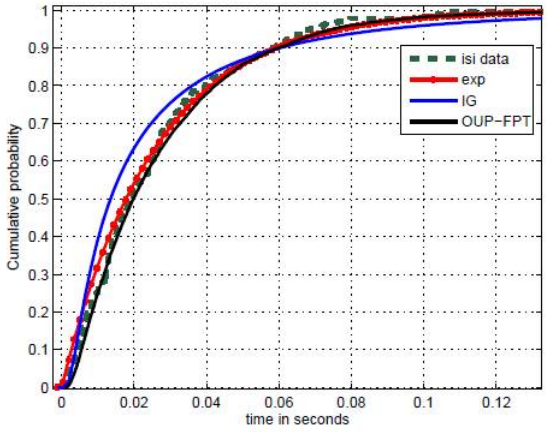

(a) Before stimulation.

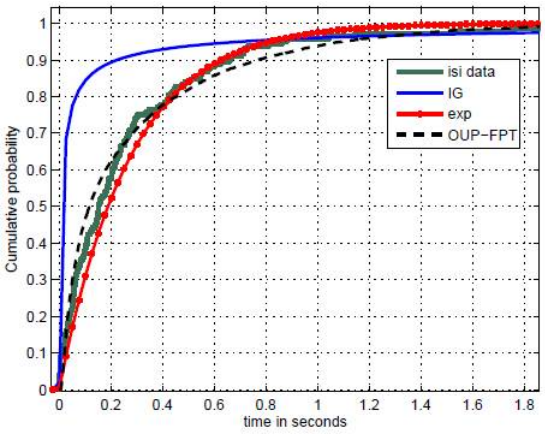

(b) During stimulation.

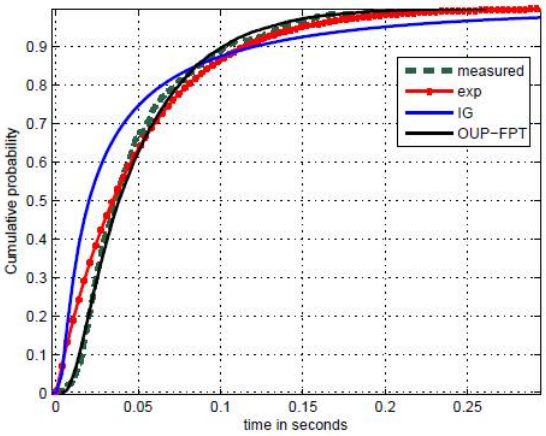

(c) After stimulation.

Figure 10. Comparison between IG, exponential and OUP-FPT CDFs fitted to the measured ISIs from the right VIM of ET patient. (a) Before applying any stimulus. (b) During a train of 160 Hz pulses for 40s. (c) Immediately after the stimulus.

CHAPTER 3

SIMULATING THE EFFECTS OF STIMULATION ON NEURONAL ACTIVITY

3.1 Including stimulation effects in the Ornstein Uhlenbeck Process model

It was shown in Chapter 2 that an OUP can be used to satisfactorily model the neuronal activity in the STN of a PD patient and in the VIM of thalamus in an ET patient. For the PD data set, neuronal recording was done in the absence of any external stimulation. In the ET data set, neuronal activity was recorded at the stimulation target both in the absence and presence of external test stimulation. In Chapter 2, it was shown that the OUP-FPT satisfactorily models the ISI distribution in general. However, during stimulation the exponential distribution performs as well as the OUP-FPT distribution. It was also shown that the set of OUP parameters during stimulation was very different from those without stimulation. In this chapter, we will account for the difference in such parameters specially the drift, μ and the diffusion, σ by using DBS parameters, current amplitude and frequency in particular.

μ and σ are the parameters in the OUP model that depend on inputs to the neuron in terms of excitatory and inhibitory impulse trains in the following way:

$$\mu = p\alpha_{\mathrm{e}}e + q\alpha_{\mathrm{i}}i; \tag{3.1}$$

$$\sigma = \sqrt{p\alpha_{\mathrm{e}}e^2 + q\alpha_{\mathrm{i}}i^2}.$$

where, α_e and α_i are rates of Poisson distributed impulses that can be excitatory or inhibitory respectively. p and q are the number of excitatory and inhibitory input dendrites respectively. The membrane potential changes by $e > 0$ or $i < 0$ depending on the type of input. Based on Equation 3.1, it can be expected that the stimulation changes μ and σ through its amplitude and frequency. If θ is the membrane time constant and assumed to be an intrinsic membrane parameter, then it should be fixed to the value used to model the neuronal activity without stimulation. However, in Chapter 2 it was seen that a higher value of θ was necessary to model the ISI distribution in the presence of stimulation. This change in θ can be due to a combination of the stimulation pulse width and the stimulation artifact which typically last for $1 - 2$ ms after each stimulation pulse. The duration of the stimulation artifact can in turn depend on the stimulation amplitude. Hence, we consider 2 values of θ: a)the value used to model ISI distribution without stimulation, b)the value in a) increased by 2 ms.

3.1.1 Modified OUP

The effect of the stimulation parameters can be included in the OUP model as follows: Let I, f be the magnitude of the stimulation current and frequency. The voltage at the recording electrode can be calculated as:

$$V = (\frac{\rho}{4\pi r} - K(f))I. \tag{3.2}$$

where ρ is the resistivity and can be set to $5000\Omega mm$ (75), $K(f)$ is a function of f to be estimated and $r = 3.6mm$ is the distance of the recording site from the stimulation site. $K(f)$

accounts for the frequency dependent capacitive impedance. The effect of I, f can be included in μ, σ as:

$$\mu_{\text{on}} = \mu_{\text{of}} - V.G(f); \tag{3.3}$$
$$\sigma^2_{\text{on}} = \sigma^2_{\text{of}} + V^2 G(f).$$

where, $\mu_{\text{on}}, \mu_{\text{of}}, \sigma_{\text{on}}, \sigma_{\text{of}}$ can be identified from ISI samples recorded with and without stimulation. $G(f), K(f)$ are functions of f which can be estimated from ISIs measured using a range of stimulation frequencies such as $120, 130, 160, 180Hz$. Thus the change in the model input parameters, μ, σ depend on the product of a function of the stimulation current and frequency. This form is motivated by the original formulation of μ, σ as in Equation 3.1. From Equation 3.2 and Equation 3.3,

$$K(f) = \frac{\rho}{4\pi r} + \frac{\sigma^2_{\text{on}} - \sigma^2_{\text{of}}}{I(\mu_{\text{on}} - \mu_{\text{of}})}; \tag{3.4}$$
$$G(f) = \frac{(\mu_{\text{on}} - \mu_{\text{of}})^2}{\sigma^2_{\text{on}} - \sigma^2_{\text{of}}}.$$

Although θ is an intrinsic parameter, from the results for the ET data set, it seems to be dependent on the stimulation. As discussed before, it can be modeled to be a function of the stimulation pulse width (p_w) and amplitude (I). Hence, it can be modeled as:

$$\theta_{\text{on}} = \theta_{\text{of}} + H(p_w, I). \tag{3.5}$$

Due to lack of data at more than one values of I, p_w, it is assumed that, $H(p_w, I) = 2ms$.

3.2 Method

3.2.1 Data Set

Data collection was done as described in Chapter 2. Neuronal activity recorded from the left VIM of thalamus of an ET patient was used. The first data set consists of recording before and during stimulation with $I = 1.5mA$ and $f = 160Hz$ and the second data set consists of recording before and during stimulation with $I = 1.5mA$ and $f = 130Hz$.

3.2.2 Parameter extraction

Using the parameter extraction method as described in Chapter 2, $\mu_{\text{of}}, \sigma_{\text{of}}, \tau_{\text{of}}$ were identified from data collected before stimulation. Similarly, $\mu_{\text{on}}, \sigma_{\text{on}}$ were identified from data collected during stimulation with $\theta_{\text{on}} = \theta_{\text{of}}$ and/or $\theta_{\text{on}} = \theta_{\text{of}} + 0.002s$. Then using Equation 3.4, $K(130), K(160), G(130), G(160)$ were calculated. Since we just have two data points for $K(f)$ and $G(f)$, a linear function of f were calculated for both K and G as:

$$\begin{aligned} G(f) &= G(130) + \frac{G(160) - G(130)}{30}(f - 130); \\ K(f) &= K(130) - \frac{K(130) - K(160)}{30}(f - 130). \end{aligned} \tag{3.6}$$

where, $f \in [130, 135, 140, 145, 150, 155, 160]$ Hz.

3.2.3 Possible metrics for evaluation of optimum stimulation parameter(s)

For each value of f, $\mu_{\text{of}}, \sigma_{\text{of}}, \mu_{\text{on}}, \sigma_{\text{of}}$ were calculated using Equation 3.3 for $I \in [1, 1.5, 2.5, 3, 3.5]$ mA. The corresponding OUP-FPT distribution was simulated (71) and the following were calculated:

1. The mean firing rate (F_{mean}): $F_{\text{mean}} = 1/E[f_{\text{ou}}]$, where $E[f_{\text{ou}}]$ is the mean of the OU-FPT distribution.
2. The ISE between OU-FPT (f_{ou})and an exponential distribution (f_{ex}) where, $f_{\text{ex}} = F_{\text{mean}} \text{e}^{-xF_{\text{mean}}}.1_{[x \geq 0]}$, x denoting the bin centers at which the distribution is calculated.
3. Entropy of ISI distribution (H_{isi}) calculated as: $H_{\text{isi}} = -\sum_i p_i log(p_i)$, where p_i is the probability of the ISIs in the $i-th$ bin.

A better stimulation might correspond to a lower mean firing rate (7) and/or a lower value of ISE (neuronal dynamics driven towards a Poisson Process)and/or a lower value of entropy (76).

3.3 Results and Discussion

Figure 11 shows $G(f), K(f)$ as a function of frequency. $G(f)$ is proportional to f in the range of frequency considered here, which is typically the therapeutic range. $K(f)$ on the other hand is inversely proportional to f. This is because $K(f)$ accounts for the frequency dependent component of capacitive impedance which is inversely proportional to frequency. With just two data points, any function could be fit to $G(f), K(f)$. A linear function was fitted for simplicity. Figure 12 shows a bunch of OUP-FPT distributions simulated for $I = 1.5mA, \theta_{\text{on}} = 0.011s$

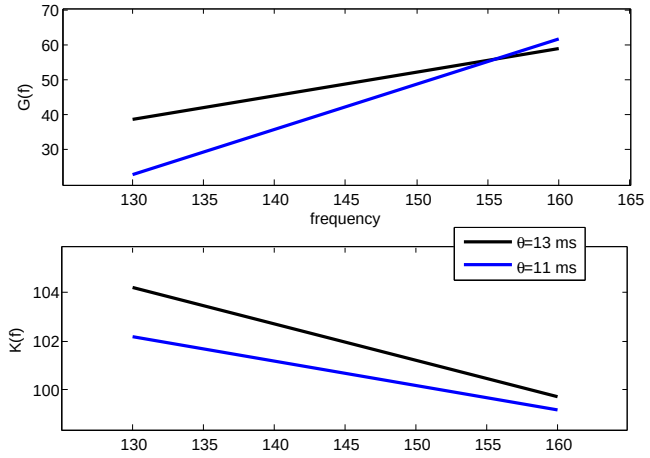

Figure 11. $G(f) \propto f$ as a linear function of f (top), $K(f) \propto 1/f$ (bottom).

(left) and $I = 3mA, \theta_{\text{on}} = 0.013s$ (right) at different frequencies. The distributions tend to get a higher peak value at a smaller ISI value as f is increased as well as I increases. This might indicate that a higher amplitude and higher frequency tends to drive the neuron to fire more frequently at a steady rate.

Figure 13(a) shows the mean firing rate (F_{mean}) (left) and the ISE between the simulated OUP-FPT and exponential distribution (right) for different set of stimulation parameters. If we consider that a lower mean firing rate corresponds to a better state, then only the first three set of parameters: $I = 1 - 1.5mA, f = 130 - 160$ would produce a mean firing rate thats lower than without stimulation. Increase in f also shows an opposite effect on the mean firing rate for $I = 1 - 1.5mA$ and $I = 2.5 - 3mA$, while for $I = 3.5mA$, increasing f first increases F_{mean} and

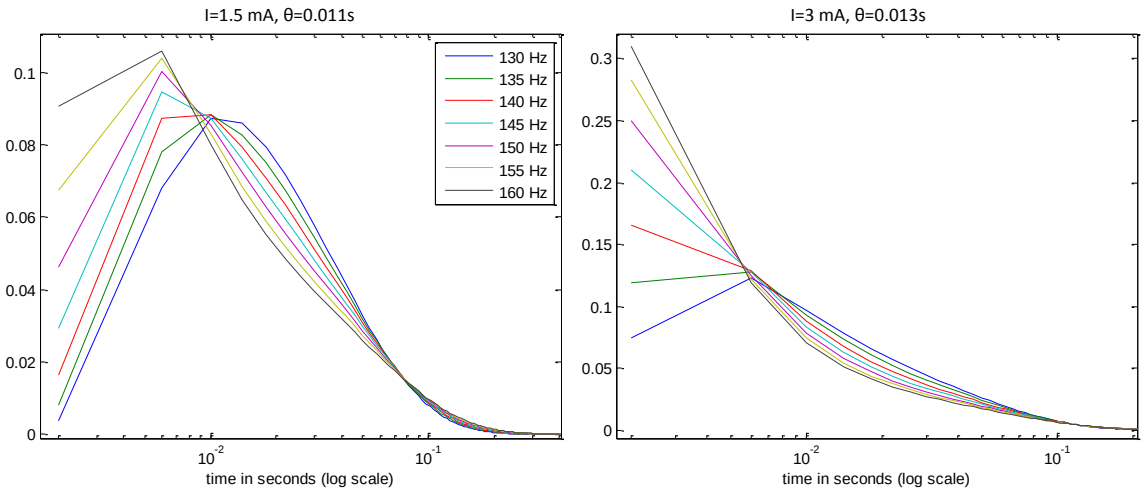

Figure 12. The OU-FPT distribution with two sets of stimulation parameters. The time axis (x-axis) is shown in the logarithmic scale.

then reduces it. From Figure 13(a) and all the parameter sets considered, $I = 1mA, f = 160Hz$ would produce the lowest value of F_{mean}. On the other hand, if a lower value of ISE corresponds to a better state, then higher I and lower f or higher f and lower I would be more optimal. The set $I = 3.5mA, f = 130Hz$ attains the lowest ISE value amongst all the sets considered. A lower ISE would mean that the spike arrival times during DBS can be assumed to follow a Poisson process. This might indicate that DBS eliminates burst firing rather than just reducing the average firing rate. Figure 13(b) shows that a high current and higher frequency produces lower values of entropy.

The OUP can be modified to include stimulation effects. One way of doing that was proposed in this chapter. Some preliminary simulation results were shown. In order to determine an optimal set of stimulation parameters, we should have neuronal recordings at atleast 3 to 4 stimulation frequencies in order to determine $K(f), G(f)$. We also should have a good cost function to determine which value of the cost function corresponds to a therapeutic state.

This can be determined be assessing the patient during stimulation at different frequencies and current amplitudes. Here, we used three metrics based on literature and results in previous section. This metric will potentially be patient specific.

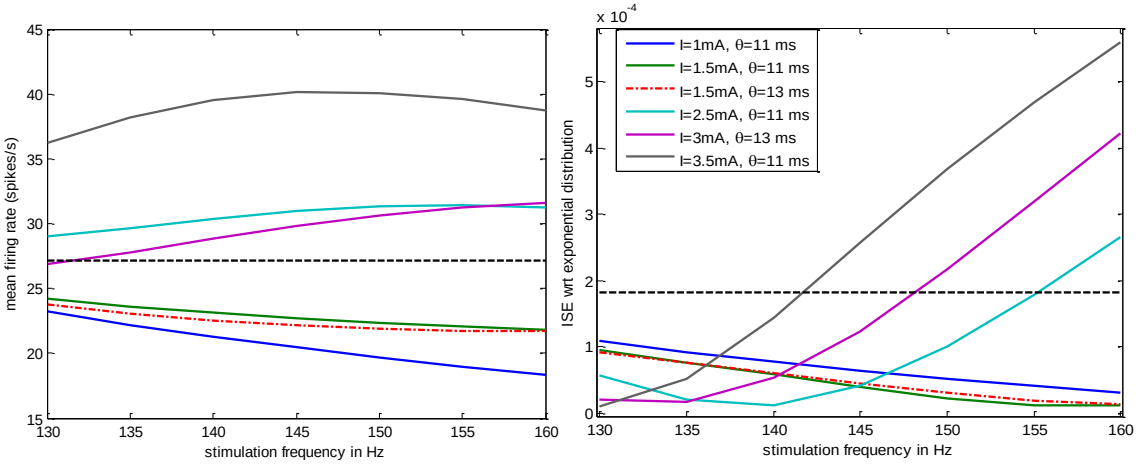

(a) F_{mean},ISE.

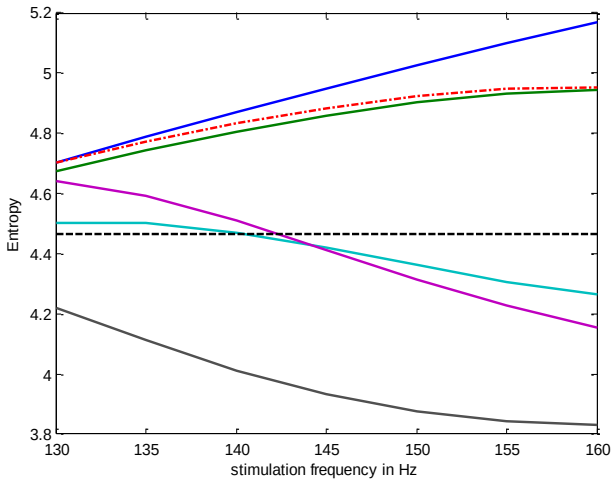

(b) H_{isi}.

Figure 13. Possible performance metrics for determining optimal stimulation parameters (frequency, current amplitude). (a) Mean firing rate (left) and ISE with respect to exponential distribution (right) for OU-FPT simulated for different sets of stimulation parameter. (b) Entropy of OUP-FPT distribution. The black dashed line shows the corresponding values before stimulation.

CHAPTER 4

ADAPTIVELY CONTROLLING DBS VIA SURFACE EMG AND ACCELERATION SIGNALS

The content of this chapter has been published in neurological research, proceedings of the 32nd Annual International Conference of the IEEE Engineering in Medicine and Biology Society (77; 23) and has been submitted for publication in the IEEE transactions on neural systems and rehabilitation engineering

4.1 Background and motivations

In this chapter, we discuss an algorithm for predicting tremor onset during a DBS-OFF period. This is required for the design of an automatic and self-adaptive ON-OFF control for DBS in PD and ET. For this to be feasible, it is necessary that:

- After the cessation of a DBS-ON period (train or packet of HFS pulses), there would exist an interval of reasonable DBS-OFF duration that is tremor-free before tremors re-appear.
- There must be a means to predict a tremor event during the DBS-OFF period, before it actually re-appears, in order to switch stimulation back on, as is essential for smooth tremor-free control.
- The information to facilitate this prediction should, if at all possible, be noninvasive, fast and simple to retrieve.

A natural choice for a non-invasively acquired signal that could be an indicative of the presence or absence of tremor is sEMG and acc mesured from tremor-affected extremities of a patient. It has been shown that thalamic cells have tremor frequency firing patterns that are linearly related to sEMG signals during tremor in ET (78).

4.1.1 Surface EMG

Surface Electromyography (sEMG) is a technique to measure muscle activity noninvasively using surface electrodes placed on the skin overlying the muscle (79). sEMG differs from needle EMG (nEMG) and fine-wire EMG (fwEMG) with respect to technical requirements and electrical properties. nEMG examines only a small muscle volume, as for a muscle biopsy. Such a sample is not necessarily statistically indicative of the general state of the muscle, and large differences may be observed between two sites in the same muscle (80). Unlike nEMG, sEMG electrodes record from a wide area of muscle territory, have a relatively narrow frequency band (20–500 Hz), have low-signal resolution, and are highly susceptible to movement artifact. Thus single fibre EMG, nEMG, macro EMG, and sEMG examine areas that are progressively larger, and the measurements become decreasingly selective and increasingly representative. sEMG electrodes typically are approximately 10 mm in diameter and usually are passive (i.e., they are simple conductive surfaces requiring low skin resistance). They can, however, be active, incorporating skin resistance and improve the signal-to-noise ratio (SNR). sEMG can record both voluntary and involuntary muscle activity in addition to externally stimulated muscle action potentials such as motor evoked potentials after central or peripheral nerve stimulation.

sEMG has been successfully used as the information source for closed-loop control in several other areas of medicine, such as control of high-above-elbow prostheses (81), electrical stimulation in paraplegics (82), and to predict the onset of sleep apnea events (83).

4.1.2 Acceleration

An accelerometer is a sensor, or transducer, which generates an electrical signal in response to acceleration (or deceleration) (84). A piezoelectric accelerometer employs either natural quartz crystals or man-made polycrystalline ceramics as its sensing element (85). Frequency and amplitude related variables extracted from acceleration (acc) signals are widely used for quantifying physiological as well as pathological tremor (86; 87).

4.1.3 Past Work

The design of a closed-loop DBS controller has been a highly pursued field over the past decade because of the fact that although the current paradigm is highly successful, it is not adaptive to the patients' condition. Research towards this goal (88) is mainly concentrated in optimizing the stimulation pattern, such as phase resetting and delayed feedback (89; 26), feedback using local field potential (LFP) and neuronal activity (75) and on using a pulse train with random frequency (43). However the results of these efforts are solely based on computational models and, if tested on human subjects, would require measurement of neuronal signals from the implant site in the brain. There has also been trials on non-human primates, where the neuronal activity from the motor cortex and Gpi were used as feedback (90). The design of a device for generating the phase resetting stimulation (89; 91), requires measurement of neuronal signals from the brain. Measuring the brain activity would require redesigning/updating the

stimulation electrodes. For this reason, our initial approach to the design of a closed-loop DBS system is to avoid measuring signals from the brain.

Our approach consists of first updating the existing FDA approved DBS system by using non-invasively measured signals, such as sEMG and acc, as feedback signals to predict re-emergence of tremor when DBS is OFF. Since this does not modify the actual stimulation generator, it can be used with the existing system as well as with future systems. We showed that the lower frequency bands of the sEMG signal, reconstructed by using a discrete wavelet transform, contains predictive information about tremor re-appearance in an ET patient with DBS implants, after the stimulation is switched OFF (23). We also showed that by using a combination of two types of entropy measures, tremor onset could be successfully predicted from sEMG recordings from an ET patient (77). Both these work were based on limited number of trials recorded from one ET patient. The use of wavelet coefficients (23) and entropy measures (77) were sufficient to predict tremor for those few trials.

4.1.4 Main contributions

A tremor prediction algorithm for closed-loop ON-OFF control of DBS is proposed. The predictor must achieve the following objectives:

- Goal 1: Tremor onset should be predicted just a few seconds before it is actually detected so that the patient does not experience any discomfort due to tremor.
- Goal 2: Voluntary movement and posture initiation in the absence of tremor should not be predicted as tremor.

This will produce a novel add-on system to the existing DBS device, that will turn the stimulation ON for a fixed time interval, switch it OFF and track a set of parameters calculated from the sEMG and acceleration in real time. It will automatically turn the stimulation back ON before the patient experiences any discomfort due to tremor such that the tremor-free DBS-OFF duration is maximized.

The algorithm uses a set of parameters extracted from sEMG and acc signals to predict tremor onsets. The designed prediction algorithm successfully predicts tremor (Goal 1) during DBS-OFF period for all the trials considered (with data collected from human subjects). At the same time it does not predict too early (Goal 2) for 80.2% of the PD trials and 85.7% of the ET trials.

4.2 Parameter Definition

In this section, parameters that will be extracted from sEMG and acc signals are defined. These parameters will be used as inputs to the tremor predictor.

4.2.1 Spectral measures

Consider a time series $x(t)$, $t \in \{1, ..., L\}$, $L = Tf_s$ where f_s and T are the sampling rate and time duration of $x(t)$, respectively. Let P_k be the power of $x(t)$ at frequency bands centered around f_k, $k \in \{1, ..., N\}$ calculated by using a Fourier transform, where $f_N - f_1$ is the signal bandwidth. Furthermore, let $x(t)$ be decomposed into M frequency bands using a discrete wavelet transform (DWT), with $x_j(t)$ representing $x(t)$ in the j-th frequency band, $j \in \{1, ..., M\}$. Then the following parameters are calculated.

1. Mean Frequency:

$$F_{\text{mean}} = \frac{\sum_{k=1}^{N} f_k P_k}{\sum_{k=1}^{N} P_k}. \tag{4.1}$$

This is a commonly used sEMG parameter (92) and represents the expected value of the frequency distribution over the spectrum range considered.

2. Power at peak frequency: Let $B < N$ where f_B represents the highest frequency content of the time series $x(t)$ and therefore $f_B - f_1$ is the bandwidth of interest. Define

$$j^\star = \arg \max_{j \in \{1,\ldots,B\}} \{P_j\}, \tag{4.2}$$

as the index of the frequency with maximum power in the bandwidth of interest. We define the power (P_{max}) at peak frequency (F_{max}) as

$$P_{\text{max}} = \frac{P_{j^\star}}{\sum_{j \in \{B+1,\ldots,N\}} P_j}, \tag{4.3}$$

$$F_{\text{max}} = f_{j^\star}. \tag{4.4}$$

The meaning of these quantities is as follows. The low frequency contents of the sEMG and acc signals are of interest as tremor components are expected to lie in this band. Let f_B represent an estimate of the highest frequency content of interest (for example, for the sEMG and acc signal f_B is around 18Hz). F_{max} is the frequency with the largest power within the bandwidth of interest, while P_{max} is the power at F_{max}. Note that P_{max} (Equation 4.3) is normalized by the power of the recorded data signal outside the

main signal bandwidth of interest. This is so because the power at $F_{\max}$ must be compared over different trials/recordings, which might have significantly different power outside the range of interest. In a way, the quantity in Equation 4.3 can be interpreted as a SNR.

3. Mean power in the j-th wavelet band:

$$\overline{P_j} = \frac{1}{L}\sum_{t=1}^{L} |x_j(t)|^2. \tag{4.5}$$

$\overline{P_j}$ captures the average signal content in the j-th frequency band over an interval of duration T.

4.2.2 Entropy measures

Wavelet Entropy has been widely used for analyzing electroencephalogram (EEG) signals to measure degree of similarity between different segments of the signal (93), for detecting different events such as seizures in epileptic patients (94); it has also been used to analyze electrocardiogram (ECG) signals for detecting myocardial infarction (95). It has been shown that tremor is characterized by an increased regularity in the corresponding sEMG signal as compared to sEMG without tremor which can be captured by the *Approximate Entropy* measure (86). It has also been used for similar analysis of EEG signals (96) and heart rate signals (97). Based on these two types of entropy measures, wavelet entropy is used to capture information relating to power shifts in different frequency bands and sample entropy to quantify the regularity and complexity of a time series signal (98). These two measures are however not directly comparable.

1. The (Shannon) entropy is a measure of unpredictability and is often used to quantify the amount of order/disorder in a signal. In information theory, the entropy of a discrete random variable (RV), X is defined as (99):

$$H(X) = -\sum_{i=1}^{K} p_i \log p_i \tag{4.6}$$

where $p_i = \mathbb{P}[X = x_i]$, $i \in \{1, ..., K\}$, is the probability mass function and K is the number of possible outcomes for X. Based on Equation 4.6, the wavelet entropy at time t of the time series signal $x(t)$, indicated as $H_{\text{wt}}(t)$, is defined as follows (93):

Let $x(t)$ be first decomposed into M frequency bands, indicated as $x_j(t), j \in \{1, ..., M\}$ by using a DWT. The normalized power of $x_j(t)$ is computed as:

$$f_j(t) = \frac{|x_j(t)|^2}{\sum_{k=1}^{M} |x_k(t)|^2}, \ j \in \{1, ..., M\}. \tag{4.7}$$

At each time instant t, $\{f_j(t), \ j \in \{1, ..., M\}\}$ can be treated as a probability mass function whose entropy is given by:

$$H_{\text{wt}}(t) = \sum_{j=1}^{M} f_j(t) \log \frac{1}{f_j(t)}. \tag{4.8}$$

2. Sample entropy was developed to overcome some shortcomings of the approximate entropy statistics such as bias, relative inconsistency and dependence on the sample length (98). It is calculated as the negative logarithm of an estimate of the conditional probability that

a data series of a given length that match point-wise within a given tolerance also match when the length is increased by one. The computation of the sample entropy, denoted as $\mathrm{SpEn}(U, m, r)$, for a given time series $U = \{x(i),\ i \in \{1, ..., L\}\}$ of length L involves two input parameters m and r, which are the pattern length and the similarity criterion, respectively. $\mathrm{SpEn}(U, m, r)$ is evaluated as follows. Let $\mathbf{x}_m(i) = [x(i), ..., x(i+m-1)]$ for $i \in \{1, ..., L-m+1\}$ be a set of length m vector sequences constructed from U. The ℓ_∞ distance between two such sequences $\mathbf{x}(i)$ and $\mathbf{x}(j)$ is

$$d_\infty[\mathbf{x}(i), \mathbf{x}(j)] = \max_{k \in \{1,...,m\}} |x(i+k-1) - x(j+k-1)|.$$

Let

$$B_i^m(r) = |\{j :\ d_\infty[\mathbf{x}_m(i), \mathbf{x}_m(j)] \leq r\}| \tag{4.9}$$

for $i, j \in \{1, ..., L-m\}, i \neq j$ and let

$$B^m(r) = \sum_{i=1}^{L-m} B_i^m(r), \quad A^m(r) = \sum_{i=1}^{L-m} B_i^{m+1}(r). \tag{4.10}$$

$\mathrm{SpEn}(U, m, r)$ is then defined as:

$$\mathrm{SpEn}(U, m, r) = \lim_{L \to \infty} -\log \frac{A^m(r)}{B^m(r)}. \tag{4.11}$$

where $A^m(r)/B^m(r)$ is the conditional probability that two sequences that are similar for m points remain similar within a tolerance r at the next point. A lower $\mathrm{SpEn}(U, m, r)$ value reflects a high degree of regularity.

In the tremor prediction algorithm, sample entropy is used to overcome some of the shortcomings of estimating the conditional probability using approximate entropy as described before (98).

4.2.3 Recurrence quantification analysis

Classical spectral characteristics of sEMG have some diagnostic value for quantification of motor unit synchronization (100). Since sEMG signals are nonlinear in nature, nonlinear time-series analyses of sEMG can potentially provide additional information on the underlying motor strategies (101). Recurrence Quantification Analysis (RQA) (102) is one such efficient time-series analysis pertaining to the class of non-linear dynamics time-domain processing. It has been extensively used for analysis of sEMG for detecting hidden characteristics that cannot be detected by linear analysis (92; 101). Different variables can be extracted from a recurrence plot (103) which has been shown to correlate with synchronization in the signal and is more sensitive to changes in the degree of synchronization than linear variables such as mean/median frequency (101).

Computation of a recurrence matrix (RM) $R_{i,j}$, $(i, j) \in \{1, ..., P\}, P = L - (M - 1)\tau$, for a time-series, $x(t)$ of length L involves the following parameters

1. The embedding dimension M,
2. The time delay τ,

3. A norm $\|\cdot\|$ (which could be minimum norm, maximum norm, and Euclidean norm),

4. Radius r.

RM is then calculated as:

$$R_{i,j} = \Theta(r - D_{i,j}),\ (i,j) \in \{1,...,P\}, \tag{4.12}$$

$$D_{i,j} = \frac{\|\mathbf{x}_i - \mathbf{x}_j\|}{d_{\text{av}}},\ \mathbf{x}_i \in \mathbb{R}^M, \tag{4.13}$$

$$d_{\text{av}} = \frac{2\sum_{i=1}^{P}\sum_{j=1}^{P} D_{i,j}}{P(P-1)} \tag{4.14}$$

where, Θ is the Heaviside function and

$\mathbf{x}_i = [x(i), x(i+\tau), ..., x(i+(m-1)\tau)],\ i \in \{1,...,P\}$; is a vector of length m.

From $R_{i,j}$, the recurrence rate R is calculated as:

$$\mathsf{R} = \frac{1}{P^2}\sum_{i,j} R_{i,j}. \tag{4.15}$$

4.3 Data Collection and Signal Preprocessing

4.3.1 Subjects

Four PD and two ET patients were recruited for this study from the Movement Disorder Clinic at Rush University Medical Center and two ET patients from the University of Illinois at Chicago hospital. Patient details are listed in Table VIII. Informed consents for this study's protocol approved by the IRB of respective institutes were obtained from all patients. The four PD patients had DBS electrodes (Medtronic DBS lead model 3389) stereotactically implanted

in the STN while the four ET patients had the electrodes placed in the VIM of the thalamus. All patients had significant tremor in one or both arms and their symptoms were well controlled by a combination of stimulation and medication.

TABLE VIII

PATIENT DETAILS

Patient#	age	gender	DBS parameter			active contacts	DBS implant	hand tested
			amplitude	frequency	pulse width			
PD1	46	M	2.8 V	180 Hz	80 μs	1-0+	2008	R
PD2	45	M	2.5 V	185 Hz	60 μs	1-2-C+	2002	L
PD3	52	F	2.8 V	185 Hz	120 μs	0-C+	2004	R
PD4	60	F	2 V	145 Hz	60 μs	1-3-C+	2009	R
ET1	64	M	2 V	150 Hz	90 μs	2-C+	2002	L
ET2	67	M	1 (L), 1.4 V(R)	130 Hz	120 μs	1-C+(L), 5-6-C+(R)	2010	L,R
ET3	51	M	2.3 V	185 Hz	60 μs	9-C+	2010	R
ET4	62	F	2 V	185 Hz	90 μs	0-C+	2007	R

4.3.2 Experimental setup

All PD patients and three ET patients had one recording session each and one ET patient had two recording sessions (one for each arm) in the Neural Control of Movement Laboratory (NCML) at the University of Illinois at Chicago. On the testing day, the patients were on their usual medication and a series of sEMG recordings were obtained from the extensor digitorum communis (EDC) and the flexor digitorum profundus (FDP) of the forearm with worst tremor. For one ET patient, sEMG was recorded from both forearms (over two recording sessions).

The EDC is the muscle that produces extension at the wrist and fingers, and muscle activity in the FDP results in wrist and finger flexion. Electrode placement was determined by muscle palpation during active wrist and finger extension and flexion. Correct placement was confirmed by inspecting sEMG output on a digital oscilloscope. The recording setup was as in (86; 104). The sEMG signal was amplified (gain set to 1,000) and bandpass filtered between 20Hz and 450Hz (Delsys Inc., Boston, MA). Along with sEMG, acc data were recorded with a calibrated Coulbourn type V94-41 miniature solid-state piezoresistive accelerometer. It was taped to the hand (2 cm proximal to the middle of the first metacarpophalangeal joint). The accelerometer resolution was 0.01g. Both sEMG and acc were sampled at $f_s = 1000$Hz.

In the beginning of the experiment, the patient was comfortably seated in an upright position on a chair. A table with an adjustable height was positioned by the side of the chair and served as the supportive surface for the subject's forearm. The height of the table was adjusted to be level with the subject's hand when the wrist and fingers were extended parallel with the floor. The table served as the visual target to enable the subject to maintain the wrist in a neutral position. With DBS-ON, three trials each of 30s duration were recorded with the patient doing the following:

R: Resting, with the forearm and hand muscles completely relaxed and the hand dangling unsupported over the edge of the supportive surface.

P: Holding a posture, by maintaining the wrist and hand in a neutral, extended position while keeping it level with the table surface.

A: Performing some voluntary action/movement, such as reaching for his opposite shoulder and/or extension and flexion of the wrist.

This produced **baseline data** with DBS-ON. Figure 14 shows the sEMG and acc sensors during R and P. After that the stimulation was switched OFF for sometime and then a total of 15 to 32 trials were recorded. Each trial was of 50-100 seconds in duration and consisted of an interval with DBS-ON followed immediately by the rest of the trial interval with DBS-OFF. After stimulation was switched OFF, the first instant when tremor visibly re-appeared was noted. This was also verified using a threshold of $0.15 - 0.2mm/s^2$ on the acc data for states R and P. In state A, Figure 16 shows that sEMG bursts with tremor (bottom) consist of smaller segregated bursts within them. This feature was used to verify the instant when tremor started. PD patients were tested under all 3 conditions (R, P, A) whereas ET patients only performed P and A since none of the ET patients had resting tremor. In P and A, the posture holding/movement was initiated either before or after switching the stimulation OFF.

4.3.3 Surface EMG data pre-processing

For final analysis, only the extensor sEMG was used as by visual inspection of the data it had a higher SNR than the flexor sEMG especially in the R and P state. During A, extensor sEMG bursts are preceded by flexor bursts, hence any predictive information is expected to be in the extensor sEMG earlier than in the flexor sEMG. This was also verified by considering parameters calculated from the flexor sEMG, whose addition did not improve the algorithm's performance. The raw extensor sEMG signal (indicated as $x(t)$) was first smoothed by calculating its power over windows of 50ms (equivalent to 50 samples) duration that slid over every sample. The

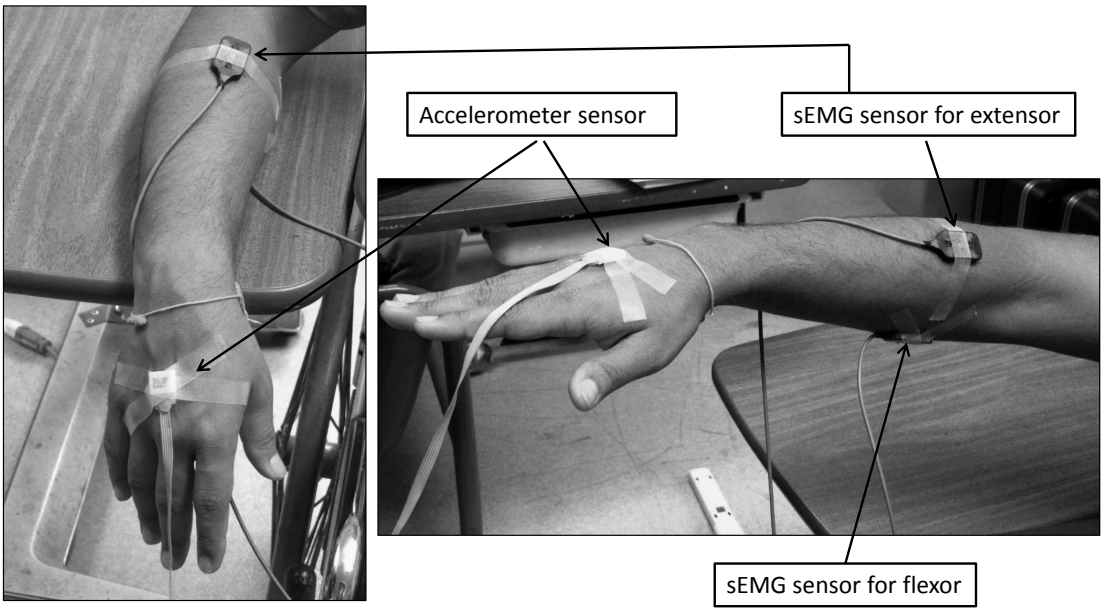

Figure 14. Hand position with sEMG and acc sensors during rest (R) (left) and posture (P) (right).

smoothed sEMG signal will be denoted as $x_s(t)$. The sEMG was smoothed to extract the lower frequency tremor bursts by averaging out the higher frequency oscillations inside the sEMG bursts. This is equivalent to rectification and low pass filtering. The following parameters as described in Section 4.2 were calculated using windows of 1s (equivalent to 1000 samples) of $x_s(t)$ with an overlap of 0.75s thus producing a sample every 0.25s after an initial delay of 1.05 s for the first parameter sample. After that,

- A 512-point Fourier transform was used to calculate the power spectral density (PSD) of each window of $x_s(t)$. Then the mean frequency ($F_{\text{mean}}^{(\text{sEMG})}$ (Equation 4.1)) and power

($P_{\max}^{(\text{sEMG})}$ (Equation 4.3)) at peak frequency ($F_{\max}^{(\text{sEMG})}$ (Equation 4.4)) were calculated for each such window. Since, the smoothed sEMG signal had most of its power concentrated in the 0-40 Hz range, only frequency components in the $2-40$Hz band were considered, that is $N = 37$ and $B = 16$ (Equation 4.4). The 0-2 Hz band was omitted to account for the DC value and very low frequency movement artifacts. $F_{\max}$ is the frequency in the 3-18 Hz range (typical tremor frequency range) with the largest power, while $P_{\max}$ is the power at $F_{\max}$.

- $x_s(t)$ was decomposed into 10 frequency bands using a Daubechies4 DWT. The mean power in the $8-16$ Hz band were computed using Equation 4.5 which will be referred to as $\overline{P_4}$. This particular band was considered because it was seen to contain the most predictive information (23) which can distinguish between tremor and voluntary movement. Moreover this band also overlaps with the typical action/postural tremor frequency band. The wavelet bands, $x_{s,j}(t)$ were also used to compute the wavelet entropy, H_{wt} (Equation 4.8).

- $x_s(t)$ was used to calculate sample entropy $\text{SpEn}(U, m, r)$ according to Equation 4.11 with $U = x_s(t),\ m = 2,\ r = 0.15\sigma$, where σ is the standard deviation (std) of the signal window considered. Since the window length $L = 1000$ should be $10^m - 30^m$ (105), $m = 2$ was chosen. For $m = 2$, values of r range from 0.1 to 0.25 times the std (97).

- $x_s(t)$ was used to calculate recurrence rate R according to Equation 4.15 with $M = 5, \tau = 3, r = 0.33$. These values were chosen based on guidelines for parameter selection outlined in the "crptool" MATLAB toolbox (106). M was estimated using the nearest-neighbor methodology, that is the minimum embedding dimension value which maximizes system

information; τ was estimated by finding the first minimum in the mutual information function and r was chosen such that $\mathsf{R} < 1$ (102).

4.3.4 Acceleration data pre-processing

The acc signal was used to calculate the mean frequency ($F_{\text{mean}}^{(\text{acc})}$ in Equation 4.1) and power ($P_{\text{max}}^{(\text{acc})}$ in Equation 4.3) at peak frequency ($F_{\text{max}}^{(\text{acc})}$ in Equation 4.4) similar to that described before for the sEMG signal $x_s(t)$.

Figures 15(a) and 15(b) show a typical PD rest trial and an ET postural trial, respectively. In each of these figures, the dashed vertical line indicates time when stimulation was switched OFF while the solid vertical line shows the time when tremor was detected visually as well as from the acc data. Note that in the postural tremor (Figure 15(b)), the posture was initiated at 40s and there is slight tremor around 50s, which becomes stronger around 80s. From the two figures, it can be easily seen that the change in sEMG power when tremor starts is more visible in the smoothed (middle) signal $x_s(t)$ than in the raw (top) signal $x(t)$. A typical action burst for a PD patient with and without tremor is shown in Figure 16, where one sees that the burst with tremor (bottom) has a more regular structure than the one without it (top). Although both have almost same number of smaller bursts (about 8) in them, the one with tremor has the bursts much more well defined and easily visible in the smoothed sEMG signal.

4.4 Prediction Algorithm

For both PD and ET, the stimulation is ON for a fixed time for each DBS ON-OFF cycle, for each patient. This fixed stimulation duration for each patient can be estimated as the DBS-ON duration that maximizes the average ratio of the delay in tremor re-appearance to

the total DBS ON-OFF duration (23). This ratio, R_{dt} is described later in Section 4.4.4. In practice, an optimum DBS-ON period can be estimated either during a patient's clinic visit or during programming of the DBS device. When the stimulation switches OFF, after this fixed duration, the prediction algorithm starts operating. Figure 17(a) shows an overall block of the signal flow for the entire prediction process.

4.4.1 Prediction Algorithm for ET

For ET patients, the prediction involves two steps:

1. **Classification of patient's state (P/A)**: This is done based on the sEMG and acc signal power by setting some thresholds as shown in Figure 17. The threshold values $[\eta_{\mathrm{c1}}, \eta_{\mathrm{c2}}, \eta_{\mathrm{c3}}, \eta_{\mathrm{c4}}, \eta_{\mathrm{c5}}, \lambda]$ for deciding the patient's state is chosen by using data during the DBS-ON interval. The following steps are done:

   i) If the power of sEMG ($x_s(t)$) over 2s just before and 1.5s immediately after stimulation is switched OFF is less than η_{c1}, then go to ii). Else the state is A.

   ii) Calculate the power of acc (indicated with P_{ac}) over 1.5s immediately after stimulation is switched OFF. If $P_{\mathrm{ac}} \in [\eta_{\mathrm{c2}}, \eta_{\mathrm{c3}}]$, the state is P. If $P_{\mathrm{ac}} < \eta_{\mathrm{c2}}$, go to iii) else go to v).

   iii) The state is R and in that case, the sEMG and acc are tracked until $acc(t_{\mathrm{vm}}) > \lambda$ where t_{vm} is the time instant when acc exceeds threshold λ.

iv) Calculate power of sEMG($x_s(t)$) over intervals $[t_{\text{vm}}, t_{\text{vm}}+0.5]$ and $[t_{\text{vm}}+0.5, t_{\text{vm}}+1]$ which are denoted as P_1 and P_2 respectively. If $P_2 < \eta_{\text{c4}}$, state is P else if $P_2 > \eta_{\text{c4}}$ and $P_1 < \eta_{\text{c5}}$, state is P. If $P_2 > \eta_{\text{c4}}$ and $P_1 > \eta_{\text{c5}}$, state is A.

v) Over the 1.5s interval after stimulation is switched OFF, find if at any instant, $\{t_{\text{vm}} : acc(t_{\text{vm}}) > 2\lambda\}$. If there is such an instant then go to iv) else the state is A.

2. **Based on the classifier output, proceed as follows.** If holding a posture (state P), the parameter ($I_{w_1=1} \times S^p_{\text{ET}}$) is tracked. If performing an action/movement (state A), the parameter ($I_{w_2=1} \times S^a_{\text{ET}}$) is tracked as shown in Figure 17(b). Here I is the indicator function, w_1 and w_2 are weights and can either be 0 or 1. $S^p_{\text{ET}}, S^a_{\text{ET}}$ are the set of parameters as described in Table IX and are a subset of the parameters introduced in the sEMG and acc data analysis in Section 4.3. Whenever, one of the parameters in S^p_{ET} (for P) or S^a_{ET} (for A) meets its corresponding prediction criterion or the DBS-OFF time exceeds a preset value, the stimulation is turned ON. The two sets of parameters and their corresponding prediction criterion are tabulated in Table IX. A description of the threshold values used in the prediction criterion are listed in Table XI. A default preset value is a safety measure to ensure that the stimulation turns ON after sometime in case the algorithm does not predict any tremor event. This value can be decided based on the average time the tremor takes to come back for a particular patient.

4.4.2 Prediction Algorithm for PD

For PD, the prediction is done similarly to that proposed for ET. The main difference is that there is no preceding classification step as in ET and a set of parameters extracted from the acc signal is also used in the prediction along with those extracted from the sEMG signal (S_{PD}). Omission of a state classification is to avoid confusion between rest tremor and change in state from R to P/A. Moreover, state classification would also require three sets of parameters for the three states in PD, thus further complicating the algorithm. Hence for the PD cases, 1s after stimulation is turned OFF, ($I_{w=1} \times S_{\mathrm{PD}}$) is tracked; whenever a prediction criterion is met or the DBS-OFF time exceeds a preset value the stimulation is turned ON. The set of parameters S_{PD} and their corresponding prediction criterion are tabulated in Table X.

4.4.3 Classification of prediction outcomes

To analyze the prediction performance, each considered trial is classified based on the prediction outcome as follows:

As shown in Figure 18, let T_{tot} be the total duration of a trial, and t_{on} and t_{off} be the times when stimulation was switched ON and OFF, respectively. Furthermore, let t_{dt} and t_{pr} be the times when tremor was detected during the DBS-OFF period and tremor was predicted using the algorithm, respectively. The trials can be classified as:

1) Tremor Detected (TD) (Trials 1 and 2 in Figure 18): These are trials where tremor was detected over the recorded DBS-OFF period, i.e $t_{\mathrm{tr}} < T_{\mathrm{tot}}$.

- If $[(t_{\mathrm{dt}} > t_{\mathrm{pr}})$ and $(t_{\mathrm{dt}} - t_{\mathrm{pr}}) < \max(5, 0.4(t_{\mathrm{pr}} - t_{\mathrm{off}}))s]$ or $[(t_{\mathrm{dt}} < t_{\mathrm{pr}})$ and $(t_{\mathrm{pr}} - t_{\mathrm{dt}}) < 1s]$, then the algorithm successfully predicts tremor and this outcome is classified as a *true*

positive (TP).

This is a bit different from the classical TP definition, in that we require that the prediction be at most 40% of the tremor free DBS-OFF period or 5s (whichever is greater) before actual tremor reappears. This allows penalizing too early prediction outcomes. The maximum between 40% of $(t_{\text{pr}} - t_{\text{off}})$ and 5s is considered to account for trials where the tremor delay is very short $(< 10s)$ for which a prediction 5s ahead in time is good enough to be classified as a *TP*. We also allow for prediction at most 1s after detection. This will take care of situations when the tremor re-appears almost immediately (within 1-2 seconds) after stimulation is switched OFF.

- If $[(t_{\text{dt}} > t_{\text{pr}})$ and $(t_{\text{dt}} - t_{\text{pr}}) > \max(5, 0.4(t_{\text{pr}} - t_{\text{off}}))s]$, then the prediction is too early and the outcome is classified as *false positive (FP).*

- If $[(t_{\text{dt}} < t_{\text{pr}})$ and $(t_{\text{pr}} - t_{\text{dt}}) > 1s]$, then the prediction is too late and the outcome is classified as *false negative (FN)*

2) No-Tremor Detected (NTD) (Trials 3 and 4 in Figure 18): These are trials where tremor was not detected over the recorded DBS-OFF interval, i.e $t_{\text{dt}} \geq T_{\text{tot}}$.

- If the algorithm does not predict any tremor over the entire interval $T_{\text{tot}} - t_{\text{off}}$, then its classified as *true negative (TN)*

- If the algorithm predicts tremor over the entire interval $T_{\text{tot}} - t_{\text{off}}$, then its classified as *false positive (FP)*

4.4.4 Analysis of prediction outcomes

For the algorithm to perform well, the total number of *TP* and *TN* must be maximized while minimizing *FP* and eliminating *FN*. This would achieve the maximum "tremor-free" DBS-OFF interval. To quantify this, the following performance metrics are defined:

$$\mathsf{A} = \frac{\#TP + \#TN}{\#TP + \#TN + \#FP + \#FN}, \tag{4.16}$$

$$\mathsf{S} = \frac{\#TP}{\#TP + \#FN}, \tag{4.17}$$

$$\mathsf{FA} = \frac{\#NTD - \#TN}{\#NTD}. \tag{4.18}$$

$$\mathsf{mcc} = \frac{(\#TP)(\#TN) - (\#FP)(\#FN)}{\sqrt{(\#TP + \#FP)(\#TP + \#FN)(\#TN + \#FP)(\#TN + \#FN)}} \tag{4.19}$$

- The parameter A in Equation 4.16 is the accuracy of the prediction algorithm, which is the ratio of the correctly predicted trials to the total number of trials. For our application, we aim to have a high accuracy (above 80%).
- The parameter S in Equation 4.17 defines the sensitivity of the prediction algorithm. It relates to the algorithm's ability to correctly predict tremor in TD trials. This value has to be very high (as close to 100% as possible) for the application since we want to avoid missing any tremor event.
- The parameter FA in Equation 4.18 is the false alarm rate, which expresses the ratio of NTD trials that are falsely predicted. This relates to the algorithm's ability to correctly identify the absence of tremor when there is no tremor. We aim to have a low FA value so that the tremor-free DBS-OFF interval is maximized.

- The parameter mcc in Equation 4.19 is the Matthews correlation coefficient (107), which is a measure of the quality of a binary classifier. It is generally regarded as a balanced measure and is used even if the classes are of very different sizes. It has a value in the range -1 to 1, where 1 represents a perfect prediction, 0 no better than random prediction and -1 indicates total disagreement between prediction and observation. It is related to the chi-square statistic for a 2×2 contingency table

$$\chi^2 = N \times \mathsf{mcc}^2 \tag{4.20}$$

  where the χ^2 statistic can be used to calculate the p-value in order to accept/reject the null hypothesis that the predictions were completely random. The p-value is the probability that $X > |\chi^2|$, where X is a random variable with a χ^2 distribution with 1 degree of freedom. A p-value less than α indicates the the prediction outcome is significantly different from a random prediction with α being the significance level and is often chosen to be 5% or less .

For this application, S should be very high (over 90%) because we want to avoid missing any tremor event. At the same time, a high A and a low FA are desired. This ensures that the algorithm not only correctly predicts tremor events, but also avoids early predictions. The mcc value should be close to 0.5 or higher and should produces a p-value that is less than 5%. Additionally, three ratios are defined as:

$$R_{\mathrm{pd}} = \sum(t_{\mathrm{pr}} - t_{\mathrm{off}}) / \sum(t_{\mathrm{dt}} - t_{\mathrm{off}}), \tag{4.21}$$

$$R_{\mathrm{dt}} = \sum(t_{\mathrm{dt}} - t_{\mathrm{off}}) / \sum(t_{\mathrm{dt}} - t_{\mathrm{on}}), \tag{4.22}$$

$$R_{\mathrm{pt}} = \sum(t_{\mathrm{pr}} - t_{\mathrm{off}}) / \sum(t_{\mathrm{pr}} - t_{\mathrm{on}}), \tag{4.23}$$

where the summation is over all the trials for each patient. R_{dt} and R_{pt} are calculated for trials where the stimulation on duration $(t_{\mathrm{off}} - t_{\mathrm{on}}) < 55$s while R_{pd} is calculated for all trials. Since for the NTD trials the exact time when tremor would come back is not known, we set $t_{\mathrm{dt}} = T_{\mathrm{tot}}$ and $t_{\mathrm{pr}} = \min(T_{\mathrm{tot}}, t_{\mathrm{pr}})$. In a practical scenario, T_{tot} would be the time when the stimulation switches ON automatically in the absence of a prediction. Hence, to determine the fraction of time the stimulation is OFF, we can consider $T_{\mathrm{tot}} - t_{\mathrm{off}}$ to be the time interval when stimulation is OFF for NTD trials.

Furthermore, R_{pt} is calculated only for trials where the DBS-ON duration, $T^*_{\mathrm{on}} = (t_{\mathrm{off}} - t_{\mathrm{on}})$, is the one that maximizes the ratio

$$R^* = \frac{t_{\mathrm{dt}} - t_{\mathrm{off}}}{T^*_{\mathrm{on}}}.$$

denoted as :

$$R^*_{\mathrm{pt}} = \frac{t_{\mathrm{dt}} - t_{\mathrm{off}}}{t_{\mathrm{pr}} - t_{\mathrm{off}} + T^*_{\mathrm{on}}}. \tag{4.24}$$

R_{pd} is the ratio between the predicted delay to the actual delay in tremor, hence R_{pd} provides a measure of how good the prediction is, i.e., a higher value indicates that the predicted delay is closer to the actual delay which is desirable. In a similar way, R_{dt} and R_{pt} provide a measure

of the fraction of time the stimulation is OFF with an ideal predictor (which would predict the exact time when tremor re-appeared) and the one designed. R_{dt} values can be used to assess if a particular patient is well suited for this type of application. If R_{dt} is very low, i.e., if the stimulation is OFF for just 10% of the total time then it is better just to have DBS-ON continuously. R^*_{pt} provides a measure of the fraction of total trial time that the stimulation would be OFF if the predictor worked only for the optimum stimulation duration, T^*_{on} . The goal of our tremor predictor is to maximize R_{pd} as well as R^*_{pt} since with a higher R^*_{pt}, the patient will have a high percentage of "tremor-free" DBS-OFF interval. T^*_{on} can be chosen as outlined in (23).

4.5 Results and Discussion

4.5.1 Parameter selection

For both PD and ET trials, the prediction parameter thresholds are listed in Table XII and Table XIV, respectively. The classification parameters for ET are listed in Table XIII. The prediction parameter thresholds were decided as follows: For each patient, all parameter values as described in Section 4.3 were first calculated for the baseline data and for the training trials (around 40% of the total trials as in Section 4.3.2). The calculated parameters for intervals of no tremor (in baseline and training trials) were compared with those in the training trials when tremor started to build up. Based on the difference between the parameter values with and without tremor, a threshold was decided for each parameter such that each of the training trial produced a desired prediction output (TP or TN). Only those parameters were included in the

set as in Table XII and Table XIV, which produced desired output for the maximum number of training trials using the same threshold.

4.5.2 Prediction performance

Based on the prediction time t_{pr}, each trial was then classified as described in Section 4.4.4. For each patient, $\mathsf{A}, \mathsf{S}, \mathsf{FA}$ in Equation 4.16, Equation 4.17, Equation 4.18; $R_{\mathrm{pd}}, R_{\mathrm{pt}}, R_{\mathrm{dt}}$ in Equation 4.21, Equation 4.23, Equation 4.22; and mcc in Equation 4.19 were calculated as in Table XV. For patients with NTD<5, FA was not calculated (NC). An overall $\mathsf{A}, \mathsf{S}, \mathsf{FA}$ and mcc were calculated based on all trials in PD and in ET shown shown in Table XV. Table XVI shows some of the trials for ET1 and PD1 with the corresponding DBS-ON time ($t_{\mathrm{off}} - t_{\mathrm{on}}$), actual tremor delay detected ($t_{\mathrm{dt}} - t_{\mathrm{off}}$), predicted delay ($t_{\mathrm{pr}} - t_{\mathrm{off}}$), total trial duration T_{tot}, and the prediction outcome classification (*TP,FP,TN,FN*).

Table XV shows that the predictor does not miss any tremor event ($\mathsf{S} = 100\%$) and that it achieves a high accuracy ($\mathsf{A} > 80$) for 6/8 patients. Out of the 8 patients, PD1 and PD3 had high tremor amplitude with a lower value of R_{dt}, as is also reflected from the values of NTD. For both of them the A, S is quite high, which is desirable. PD4 was the only PD patient who had long delays in tremor with 11/32 NTD trials. The lower A and relatively high FA is because of the fact that the algorithm predicted a tremor either in the NTD cases or predicted a tremor too early for the TD cases. PD2 had moderate tremor amplitude and all the FP's except one are due to early prediction in the TD cases. ET3 and ET4 had almost no tremor during holding a posture but had tremor while performing an active movement. ET2 had very low amplitude tremor on the right hand. The FA could not be calculated for every patient

because some of them had very few or no NTD trials. Hence an overall FA value was also calculated for ET and PD by considering all ET and PD trials respectively. It should be noted that for this application, we aim to achieve S as close to 100% as possible. Hence, for patients who have relatively higher delays in tremor re-appearance and/or lower tremor amplitude, the algorithm predicts early tremor events for some of the trials resulting in a higher value of FA.

The mcc value was calculated for each patient, except PD3 due to an indeterminate form produced by $TN = FN = 0$. For all the 7 patients, the mcc value was close to or greater than 0.5 and the overall mcc for both PD and ET were above 0.5. This indicates 50% or higher correlation between predicted and actual classification for each patient(PD/ET) and for overall PD and ET trials. The mcc was further used to calculate the χ^2 test statistics according to Equation 4.20 in order to determine the corresponding p-value. Each p-value (both individual and overall) was less than $\alpha = 5\%$, which indicates that the null hypothesis that the prediction is completely random can be rejected.

4.5.3 Overall performance

The overall S for both ET and PD is 100% which means that for all TD trials in ET and PD, the predictor does not miss any tremor event during the DBS-OFF interval. The overall A for ET is 85.7% while for PD is 80.2%, which indicates that in 85.7% of all ET trials and in 80.2% of all PD trials, the algorithm correctly predicts tremor. Correct tremor prediction means that, in the TD trials, tremor is predicted not too early while in the NTD trials, tremor is not predicted. The overall FA for ET is 11.6% and for PD is 29.4%, which means that in 11.6% of the ET NTD trials and in 29.4% of the PD NTD trials, the algorithm predicts tremor.

The performance for ET is in general better than that for PD with higher overall A and lower FA because of a preceding classification step that allowed to choose different parameters for each state. A classification in PD is more challenging due to the fact that a change in power in the sEMG/acc from the rest state could either be due to tremor or movement while for ET it is certain that there is no tremor during rest and hence an increase in power is certainly due to some movement initiation which might be accompanied by tremor.

4.5.4 Practical considerations

In this study, we have shown that an adaptively controlled ON-OFF DBS can be designed as an add-on system to the existing one by using non-invasively measured sEMG and acc from the tremor affected extremities of patients with pathological tremor such as in PD and ET. The application would however be patient specific and might not be beneficial to certain patients with severe tremor and short delay in tremor, such as PD3, who had the lowest value of R_{pt}. For all other patients, $R^*_{\mathrm{pt}} > 30\%$ respectively which means that with the optimal stimulation duration, T^*_{on}, the proposed adaptive ON-OFF DBS controller achieves a "tremor free DBS-OFF period" that is greater than 30% of the total ON-OFF duration as shown by the R^*_{pt} values in Table XV. We acknowledge that this type of DBS controller specially takes into account only the tremor symptom while PD patients also suffer from rigidity and slowness of movement. However, for most PD patients who have tremor, it is the symptom that re-appears the earliest after the DBS is switched OFF (108). For ET patients, this type of DBS controller may have additional benefit beyond just extending battery life, as it has been shown that for some ET patients the stimulation benefits decrease over time (109). It was also seen that for some such

ET patients, restarting the stimulation after its temporary discontinuation resensitized them to stimulation (110). Hence lesser and discontinuous current injection might actually help in prolonging the therapeutic effects of DBS in ET.

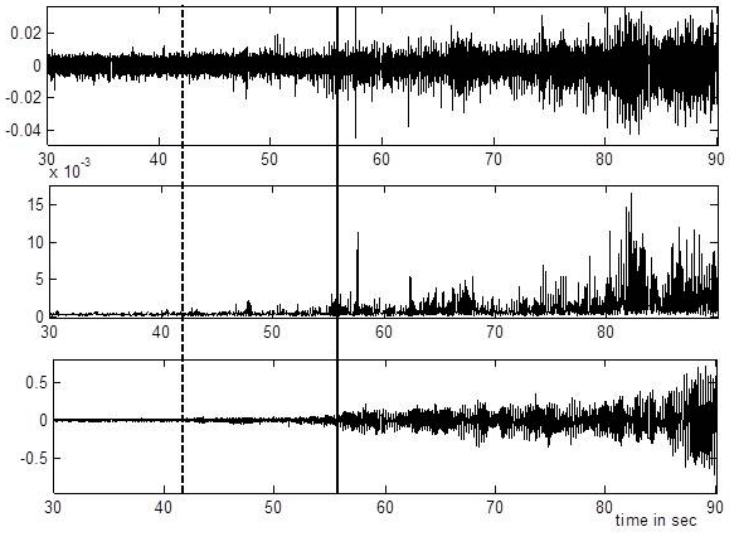

(a) PD Rest (R).

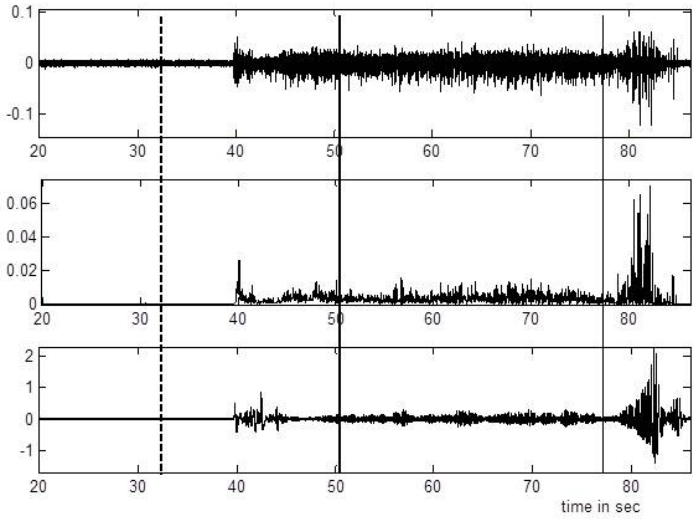

(b) ET posture (P).

Figure 15. Raw extensor sEMG (top), smoothed extensor sEMG (middle) and acceleration (bottom) recorded from (a) a PD patient at rest. (b)an ET patient while holding a posture (initiated at 40s). The dashed line shows time of turning stimulation OFF while the solid line shows the time when tremor is detected based on visual inspection as well as acceleration data. Note that at 50s, tremor was of low intensity and it increased at around 79s.

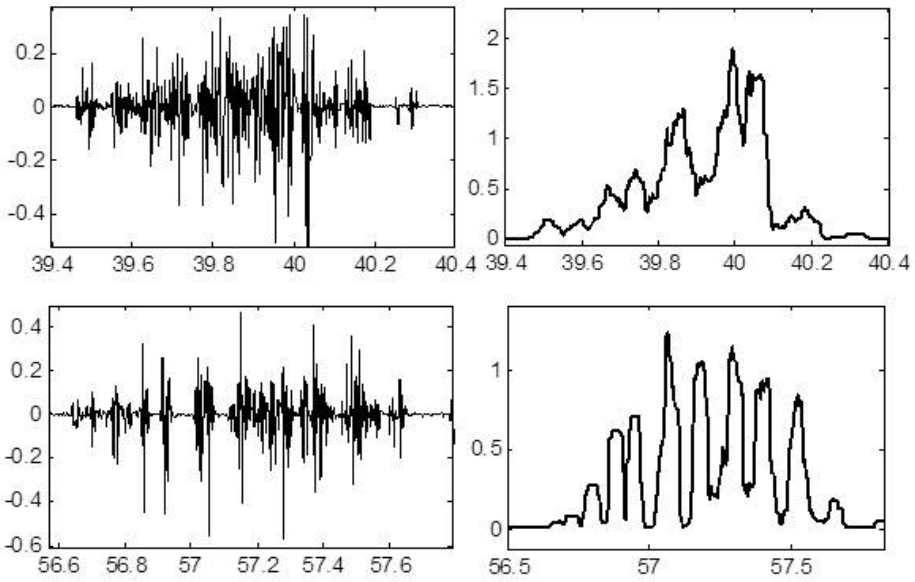

Figure 16. Raw extensor sEMG (left), smoothed extensor sEMG (right) during a voluntary movement performed by a PD patient. The top burst is without tremor while the lower one is with tremor.

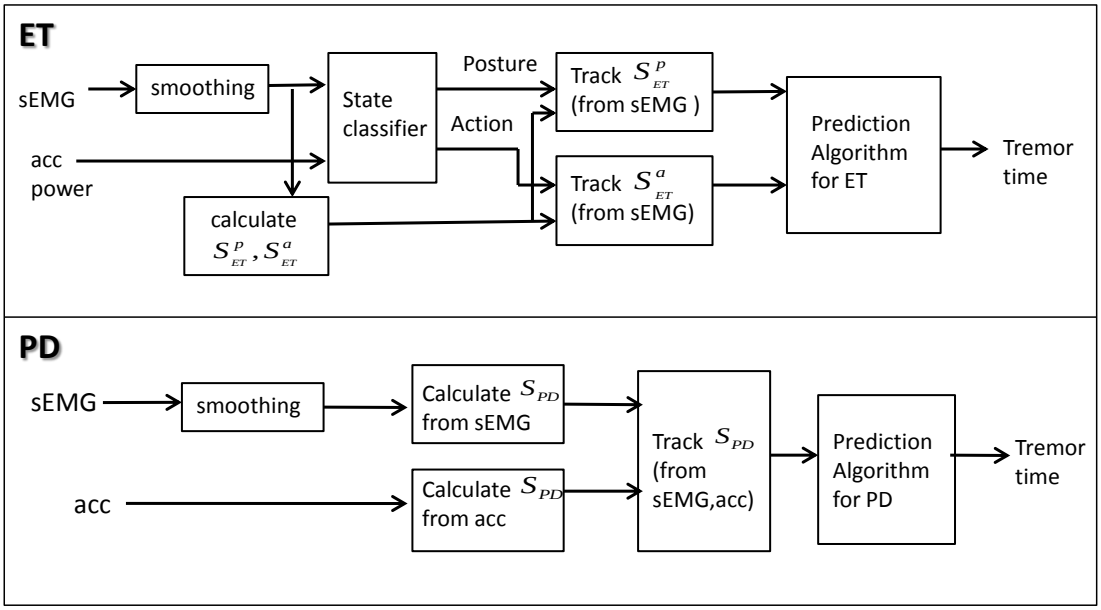

(a) Overview of signal flow.

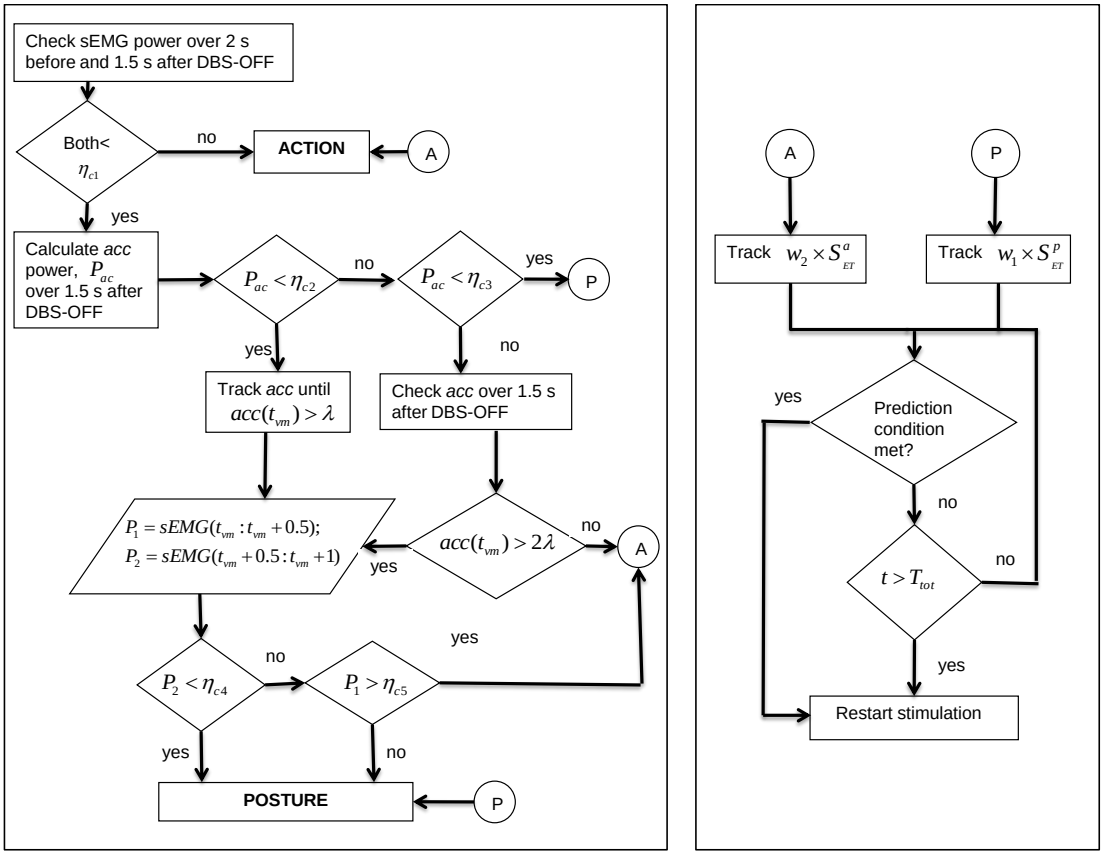

(b) Algorithm flowchart for ET.

Figure 17. (a) A block diagram showing how the two signals, sEMG and acc are used in the algorithm for ET (top) and PD (bottom) (b) Classification (left) and prediction (right) for the ET algorithm described in Section 4.4.1 and shown in (a).

TABLE IX

PARAMETER SET FOR ET.

#	**Parameter Set,** $S^{p}_{\mathbf{ET}}$	**Predict tremor at time** t
1	SpEn and $\overline{P_4}$	Let $(i-1)$ is a local min and $k<i$ is a local max over $(k-1,i)$, if $\text{SpEn}(k)\in(\eta_{\text{l}1},\eta_{\text{h}1})$ & $\text{SpEn}(i-1)\in(\eta_{\text{l}2},\eta_{\text{h}2})$ & $\overline{P_4}(l)>\eta_{\text{p}}$, $l\in(k-6,i+4)$, $\mathbf{t}=\max(\mathbf{i},\mathbf{l})$
2	R	Let $(i-1)$ is a local max and $k<i$ is a local min over $(k-1,i)$, $\mathsf{R}(i-1)-\mathsf{R}(k)\in(\rho_{\text{l}},\rho_{\text{h}})$,**t=i**
3	$P^{(\text{sEMG})}_{\max}$ and $F^{(\text{sEMG})}_{\max}$	If $F^{(\text{sEMG})}_{\max}(i)\in(f_{\text{l}},f_{\text{h}})$ and $P^{(\text{sEMG})}_{\max}(i)>f_{\text{p}}$,**t=i**
#	**Parameter Set,** $S^{a}_{\mathbf{ET}}$	**Predict tremor at time i**
1	R	Let $(i-1)$ is a local max and $k<i$ is a local min over $(k-1,i)$,$\mathsf{R}(i-1)-\mathsf{R}(k)\in(\rho_{\text{l}},\rho_{\text{h}})$, **t=i**
2	$F^{(\text{sEMG})}_{\text{mean}}$	If $F^{(\text{sEMG})}_{\text{mean}}(i)\in(f_{\text{l}},h_{\text{h}})$, **t=i**

TABLE X

PARAMETER SET FOR PD.

#	**Parameter Set,** $S_{\mathbf{PD}}$	**Predict tremor at time t**
1	SpEn & $\overline{P_4}$	Let $(i-1)$ is a local min and $k<i$ is a local max over $(k-1,i)$, if $\text{SpEn}(k)\in(\eta_{\text{l}1},\eta_{\text{h}1})$ & $(\text{SpEn}(k)-\text{SpEn}(i-1))\in(\eta_{\text{l}2},\eta_{\text{h}2})$ & $\overline{P_4}(l)>\eta_{\text{p}}$, $l\in(k-6,i+4)$, $\mathbf{t}=\max(\mathbf{i},\mathbf{l})$
2	R	Let $(i-1)$ is a local max and $k<i$ is a local min over $(k-1,i)$, $\mathsf{R}(i-1)-\mathsf{R}(k)\in(\rho_{\text{l}},\rho_{\text{h}})$,**t=i**
3	$P^{(\text{sEMG})}_{\max}$ & $F^{(\text{sEMG})}_{\max}$	If $F^{(\text{sEMG})}_{\max}(i)\in(f_{\text{l}1},f_{\text{h}1})$ and $P^{(\text{sEMG})}_{\max}(i)>f_{\text{p}1}$,$\mathbf{t}=\mathbf{i}$
4	$P^{(\text{acc})}_{\max}$ and $F^{(\text{acc})}_{\max}$	If $F^{(\text{acc})}_{\max}(i)\in(f_{\text{l}2},f_{\text{h}2})$ and $P^{(\text{acc})}_{\max}>f_{\text{p}2}$, $\mathbf{t}=\mathbf{i}$
5	H_{wt}	Let $H_{\text{wt}}(i-1)$ and $H_{\text{wt}}(i)\in(h_{\text{l}},h_{\text{h}})$, **t=i**

TABLE XI

THRESHOLD DEFINITION.

#	**Parameter**	**Thresholds**	**Description**
1	SpEn and $\overline{P_4}$	$\eta_{\text{l}1},\eta_{\text{h}1}$	lower and upper thresholds for maximum SpEn
		$\eta_{\text{l}2},\eta_{\text{h}2}$	lower and upper thresholds for minimum SpEn in ET and decrease in SpEn for PD
		η_{p}	lower threshold for $\overline{P_4}(l)$
2	R	$\rho_{\text{l}},\rho_{\text{h}}$	lower and upper thresholds for increase in R
3	$P^{(\text{sEMG})}_{\max}$ and $F^{(\text{sEMG})}_{\max}$	$f_{\text{l}},f_{\text{h}}$	lower and upper thresholds for $F^{(\text{sEMG})}_{\max}$,
		f_{p}	lower threshold for $P^{(\text{sEMG})}_{\max}$
4	$F^{(\text{sEMG})}_{\text{mean}}$	$f_{\text{l}},f_{\text{h}}$	lower and upper thresholds for $F^{(\text{sEMG})}_{\text{mean}}$
5	$P^{(\text{acc})}_{\max}$ and $F^{(\text{acc})}_{\max}$	$f_{\text{l}2},f_{\text{h}2}$	lower and upper thresholds for $F^{(\text{acc})}_{\max}$
		$f_{\text{p}2}$	lower threshold for $P^{(\text{acc})}_{\max}$
5	H_{wt}	$h_{\text{l}},h_{\text{h}}$	lower and upper thresholds for $H_{\text{wt}}(i-1,i)$

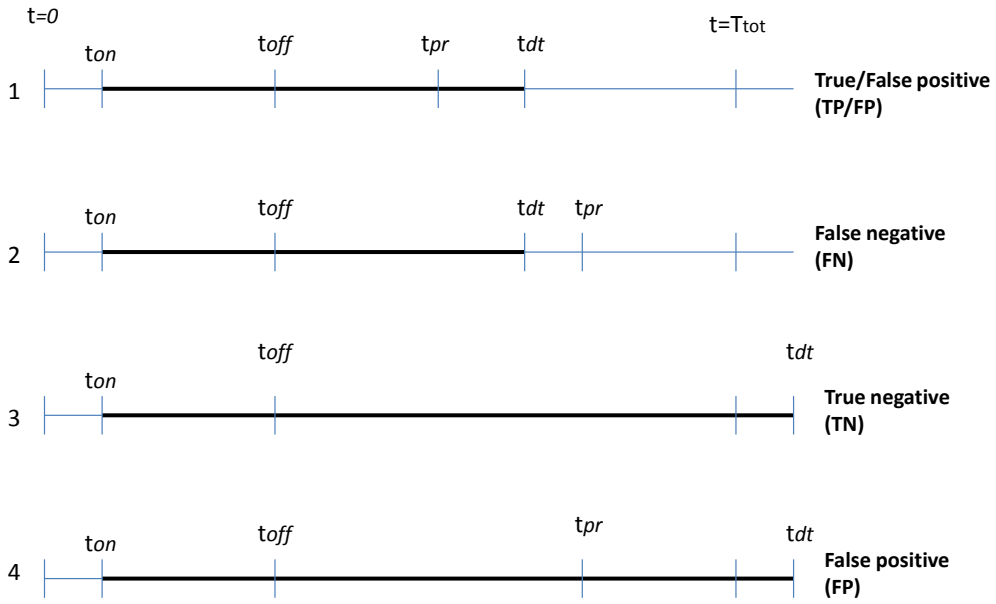

Figure 18. Timing points for events from DBS-ON time (t_{on}) to tremor detection time (t_{dt}) marked in bold line. There are 4 possible scenarios: 1,2 are TD trials, in 1 the tremor is predicted before its detection (TP/FP) and in 2 tremor is predicted after its detection (FN); 3,4 are NTD trials, in 3 tremor is not predicted over the entire interval *TN* and in 4 tremor is predicted *FP*. *Notation*: T_{tot} is the total duration of a trial, t_{on} and t_{off} are the times when DBS was switched ON and OFF respectively, t_{dt} and t_{pr} are the times when tremor was detected and predicted using the algorithm, respectively.

TABLE XII

PARAMETER THRESHOLD FOR PREDICTION ALGORITHM FOR PD.

Patient#	Parameters with $w = 1$	threshold
PD1	SpEn and $\overline{P_4}$	$(\eta_{\mathrm{l}1}, \eta_{\mathrm{h}1}) = (0.2, 0.35); (\eta_{\mathrm{l}2}, \eta_{\mathrm{h}2}) = (0.11, 0.2); \eta_{\mathrm{p}} = 15;$
	SpEn and $\overline{P_4}$	$(\eta_{\mathrm{l}1}, \eta_{\mathrm{h}1}) = (0.35, 0.4); (\eta_{\mathrm{l}2}, \eta_{\mathrm{h}2}) = (0.14, 0.34); \eta_{\mathrm{p}} = 15;$
	R	$(\rho_{\mathrm{l}}, \rho_{\mathrm{h}}) = (0.2, 0.22)$
	$P_{\max}^{\mathrm{sEMG}}$ and $F_{\max}^{\mathrm{sEMG}}$	$f_{\mathrm{p}1} = 28; (f_{\mathrm{l}1}, f_{\mathrm{h}1}) = (4, 10)$
PD2	SpEn and $\overline{P_4}$	$(\eta_{\mathrm{l}1}, \eta_{\mathrm{h}1}) = (0.2, 0.32); (\eta_{\mathrm{l}2}, \eta_{\mathrm{h}2}) = (0.1, 0.16); \eta_{\mathrm{p}} = 28;$
	H_{wt}	$(h_{\mathrm{l}}, h_{\mathrm{h}}) = (0.31, 0.35)$
PD3	H_{wt}	$(h_{\mathrm{l}}, h_{\mathrm{h}}) = (0.32, 0.36)$
	$P_{\max}^{\mathrm{acc}}$ and $F_{\max}^{\mathrm{acc}}$	$f_{\mathrm{p}2} = 30; (f_{\mathrm{l}2}, f_{\mathrm{h}2}) = (4, 7)$
PD4	SpEn and $\overline{P_4}$	$(\eta_{\mathrm{l}1}, \eta_{\mathrm{h}1}) = (0.25, 0.34); (\eta_{\mathrm{l}2}, \eta_{\mathrm{h}2}) = (0.15, 0.22); \eta_{\mathrm{p}} = 25;$
	H_{wt}	$(h_{\mathrm{l}}, h_{\mathrm{h}}) = (0.275, 0.295)$
	$P_{\max}^{\mathrm{acc}}$ and $F_{\max}^{\mathrm{acc}}$	$f_{\mathrm{p}2} = 30; (f_{\mathrm{l}2}, f_{\mathrm{h}2}) = (4, 7)$

TABLE XIII

THRESHOLD FOR STATE CLASSIFICATION IN ET.

Patient#	threshold
ET1	$\eta_{\mathrm{c}1} = 0.35, \eta_{\mathrm{c}2} = 0.6, \eta_{\mathrm{c}3} = 1.2, \eta_{\mathrm{c}4} = 0.15, \eta_{\mathrm{c}5} = 0.2, \lambda = 0.2$
ET2	$\eta_{\mathrm{c}1} = 0.06, \eta_{\mathrm{c}2} = 0.5, \eta_{\mathrm{c}3} = 3, \eta_{\mathrm{c}4} = 0.4, \eta_{\mathrm{c}5} = 0.15, \lambda = 0.2$
ET3	$\eta_{\mathrm{c}1} = 0.1, \eta_{\mathrm{c}2} = 0.6, \eta_{\mathrm{c}3} = 3, \eta_{\mathrm{c}4} = 0.07, \eta_{\mathrm{c}5} = 0.01, \lambda = 0.1$
ET4	$\eta_{\mathrm{c}1} = 0.5, \eta_{\mathrm{c}2} = 1.1, \eta_{\mathrm{c}3} = 1.6, \eta_{\mathrm{c}4} = 0.1, \eta_{\mathrm{c}5} = 0.15, \lambda = 0.2$

TABLE XIV

PARAMETER THRESHOLD FOR PREDICTION ALGORITHM FOR ET.

Patient#	Parameter with $w_1, w_2 = 1$	threshold
ET1	SpEn and $\overline{P_4}(w_1)$	$(\eta_{\mathrm{l}1}, \eta_{\mathrm{h}1}) = (0.25, 0.3); (\eta_{\mathrm{l}2}, \eta_{\mathrm{h}2}) = (0.18, 0.22); \eta_{\mathrm{p}} = 10;$
	$P_{\max}^{\mathrm{sEMG}}$ and $F_{\max}^{\mathrm{sEMG}}(w_1)$	$f_{\mathrm{p}} = 22 (f_{\mathrm{l}}, f_{\mathrm{h}}) = (5, 10)$
	$\mathsf{R}(w_2)$	$(\rho_{\mathrm{l}}, \rho_{\mathrm{h}}) = (0.3, 0.35)$
	$F_{\mathrm{mean}}^{\mathrm{sEMG}}(w_2)$	$(f_{\mathrm{l}}, f_{\mathrm{h}}) = (10, 11)$
ET2(left)	$P_{\max}^{\mathrm{sEMG}}$ and $F_{\max}^{\mathrm{sEMG}}(w_1)$	$f_{\mathrm{p}} = 20 (fl, fh) = (4, 10)$
	$\mathsf{R}(w_2)$	$(\rho_{\mathrm{l}}, \rho_{\mathrm{h}}) = (0.3, 0.4)$
ET2(right)	SpEn and $\overline{P_4}(w_1)$	$(\eta_{\mathrm{l}1}, \eta_{\mathrm{h}1}) = (0.45, 0.5); (\eta_{\mathrm{l}2}, \eta_{\mathrm{h}2}) = (0.1, 0.2); \eta_{\mathrm{p}} = 10;$
	$F_{\mathrm{mean}}^{\mathrm{sEMG}}(w_2)$	$(f_{\mathrm{l}}, f_{\mathrm{h}}) = (11, 12)$
ET3	SpEn and $\overline{P_4}(w_1)$	$(\eta_{\mathrm{l}1}, \eta_{\mathrm{h}1}) = (0.3, 0.4); (\eta_{\mathrm{l}2}, \eta_{\mathrm{h}2}) = (0.16, 0.18); \eta_{\mathrm{p}} = 50;$
	$\mathsf{R}(w_2)$	$(\rho_{\mathrm{l}}, \rho_{\mathrm{h}}) = (0.4, 0.48)$
	$F_{\mathrm{mean}}^{\mathrm{sEMG}}(w_2)$	$(f_{\mathrm{l}}, f_{\mathrm{h}}) = (11, 12)$
ET4	SpEn and $\overline{P_4}(w_1)$	$(\eta_{\mathrm{l}1}, \eta_{\mathrm{h}1}) = (0.78, 0.98); (\eta_{\mathrm{l}2}, \eta_{\mathrm{h}2}) = (0.38, 0.48); \eta_{\mathrm{p}} = 20;$
	$P_{\max}^{\mathrm{sEMG}}$ and $F_{\max}^{\mathrm{sEMG}}(w_1)$	$f_{\mathrm{p}} = 22 (f_{\mathrm{l}}, f_{\mathrm{h}}) = (5, 10)$
	$\mathsf{R}(w2)$	$(\rho_{\mathrm{l}}, \rho_{\mathrm{h}}) = (0.3, 0.34)$

TABLE XV

PREDICTION PERFORMANCE WITH RATIOS EXPRESSED IN %. *NOTE: NC MEANS NOT CALCULATED;* FA *FOR PD4 AND FOR OVERALL PD ARE NOT SAME BECAUSE ALTHOUGH* FA *WAS NOT CALCULATED FOR PD(1-3), PD(1-2) HAD A FEW NTD TRIALS WHICH WERE INCLUDED IN THE CALCULATION OF OVERALL* FA.

Patient#	NTD	*TP,TN,FP,FN*	A	S	FA (%)	R_{pd}	$R_{\mathrm{pt}}, R_{\mathrm{dt}}$	$T^*_{\mathrm{on}}, R^*_{\mathrm{pt}}$	mcc,p-value
PD1	2	14,1,1,0	93.6	100	NC	77.6	28.6,34.1	30-35,34.2	0.68,0.006
PD2	4	16,3,7,0	73.1	100	NC	67.0	28.5,37.7	20-40,31	0.46,0.02
PD3	0	15,0,2,0	88.2	100	NC	68.8	11.5,15.9	NA	NA
PD4	11	16,8,8,0	75.0	100	27.3	80.7	34.3,39.3	20-40,42.4	0.53, 0.003
All PD	17	61,12,18,0	80.2	100	29.4	NC	NC	NC	$0.56{,}9 \times 10^{-9}$
ET1	3	10,2,3,0	80.0	100	NC	80.2	35.2,40.4	20-40,37.4	0.55,0.03
ET2	14	13,14,3,0	90.0	100	0	89.8	36.8,39.3	20-40,39.1	0.82,0
ET3	6	10,5,1,0	87.5	100	16.7	79.1	32.8,38.1	30-42,32.8	0.87,0.0005
ET4	20	7,17,6,0	80.0	100	15	88.7	48.3,51.3	15-40,48.3	0.63,0.0005
All ET	43	40,38,13,0	85.7	100	11.6	NC	NC	NC	0.71,0

TABLE XVI

SOME TYPICAL TRIALS FOR PD1 AND ET1. LEGEND: R (REST), P (POSTURE), A (ACTION), ND (NOT DETECTED), NP (NOT PREDICTED).

Trial#	$t_{\mathrm{off}} - t_{\mathrm{on}}$	$t_{\mathrm{dt}} - t_{\mathrm{off}}$	$t_{\mathrm{pr}} - t_{\mathrm{off}}$	$t_{\mathrm{pr}} - t_{\mathrm{dt}}$	N	o/p type
PD1						
R1	41	14	11.5	2.5	80	*TP*
R2	31	21	17.25	3.75	70	*TP*
P1	41	18	15	3	80	*TP*
P2	31	10.5	5.5	5	70	*TP*
A1	31	ND	14.5	NA	70	*FP*
A2	31	ND	NP	NA	70	*TN*
ET1						
P1	37	30	25.75	4.25	80	*TP*
P2	28	17	4.75	12.25	70	*FP*
A1	38	ND	37.25	NA	80	*FP*
A2	23.75	28.25	26	2.25	70	*TP*

CHAPTER 5

CONCLUSION AND FUTURE WORK

5.1 Conclusion

To conclude, the following has been shown:

1. An OUP can be used to model the dynamics of a single neuron at the site of DBS electrode implantation. From the ISIs calculated from measured neuronal activity during DBS surgery, the OUP model parameters can be extracted. The simulated OUP-FPT distribution using the identified parameters was shown to follow the empirical ISI distribution closely in terms of two distance measures. The OUP provides a balance between an oversimplified model such as the PP and one involving too many parameters that require precise physiological values. The parameter θ (membrane time constant) provides flexibility to fit data recorded under different conditions (with/without external stimulation). An interesting observation is that an exponential distribution actually fits better than the OUP-FPT during DBS-ON intervals. This indicates that the spike arrival times during DBS follows a poisson process. This might indicate that the effect of DBS on neuronal firing is to make it more regular and thus eliminate burst firing.

2. The OUP model can be modified to account for the effect of external stimulation (DBS) on the neuronal firing activity. Such a model could be used to determine an optimal set of stimulation parameters which would drive the firing pattern to a more desirable state

(reduced firing rate, firing times following a Poisson process, lower entropy of the ISI distribution.).

3. Non-invasively measured sEMG and acc can be used for designing an adaptively controlled ON-OFF DBS paradigm which can be added on to the existing DBS system. A set of frequency related and entropy type parameters can be used to successfully predict a tremor event during a DBS-OFF interval, before it becomes a discomfort for the patient. The PD prediction algorithm does not include a preceding state classification as in the one for ET. The algorithm also requires determining the optimal set of parameters and setting their thresholds for each patient which requires some training and manual intervention.
4. By combining the two parts, a new DBS paradigm can be established which does not require changing the FDA approved electrode or pacemaker design. The optimal stimulation parameters during DBS-ON period can be determined using the proposed model. During DBS-OFF period, muscular and kinematic signals can be used for predicting an incoming tremor event. This information can be wirelessly transmitted to the implanted pacemaker from sEMG/acc sensors implanted on the tremor affected muscles.

5.2 Future Work

This work opens up the following interesting directions of future research:

1. Determining optimal DBS parameters from the model of neuronal activity.
2. Adapting parameters of the tremor prediction algorithm over time.
3. Use of both neuronal activity and sEMG/acc for DBS ON-OFF control.

5.2.1 Optimal DBS parameters

It was shown in Chapter 2 that an OUP can be used to satisfactorily model the neuronal activity in the STN of a PD patient as well as the one in the VIM of thalamus in an ET patient. However, this needs to be tested on more patient data which solely depends on the number of PD and ET patients undergoing surgery for DBS. Since it is not possible to measure the membrane potential of a single neuron extracellularly, we can only estimate a model governing its dynamics and identify parameters from observable events such as spike generation.

It was also shown in Chapter 3 that the effects of the stimulation parameters (amplitude and frequency) can be included in the OUP model. More work needs to be done in this direction which are as follows:

1. In order to satisfactorily estimate the function $K(f), G(f)$, recordings at 4-5 frequencies need to be done.
2. A good metric to indicate a therapeutic state needs to be determined as this is crucial for determining the optimal set of stimulation parameters.
3. To include the stimulation pulse width into the model, recordings using atleast 3-4 stimulation pulse width is required.
4. Effects on the LFP spectrum can also be determined by simulating LFPs with and without DBS can by aggregating over a neuronal population distributed over a sphere centered around the recording tip (75).

A wide range of stimulation parameters can be used to simulate neuronal activity (single cell firing and/or LFP). An optimal set of DBS parameters can be determined as the one that drives the simulated neuronal dynamics to the desired state. This desired state can be a reduced firing rate, reduced variability (low entropy) of the ISI distribution or a reduction in the LFP power in certain low frequency bands (7). This will thus help determine an optimal stimulation strategy.

Another direction of future work would be to use a more optimal OUP parameter identification strategy which takes into account the entire distribution rather than just the first two moments as was used in this work.

5.2.2 Adaptively modifying tremor prediction thresholds

It was shown that sEMG and acc recorded from a patients with ET and PD have features that allow predicting onset of tremor to facilitate starting of a next stimulation packet before tremor reappears. This establishes the feasibility of sEMG/acc-based predictive ON-OFF control of DBS in certain ET and PD patients. However, the proposed tremor prediction algorithm depends on one or two threshold(s) for each parameter used. These thresholds were determined based on some training data and were fixed for all the trials considered. Since, both ET and PD are progressive disorders, it is expected that these thresholds would change over time. Hence they need to be recalibrated after certain periods of time. Hence an interesting direction of future work would be to adapt the thresholds automatically based on signals measured during the DBS-ON periods. Another alternative would be to use a neural network type predictor (111) for the tremor prediction which can train itself over regular intervals of time.

The PD prediction algorithm does not include a preceding state classification as in the one for ET. Hence designing a 2 or 3 state classifier preceding the predictor might improve prediction results for PD patients.

5.2.3 Use of multiple signals for control

Neuronal activity in the form of single cell recordings have only been considered. However such signals are accessible only during surgery. Hence, although it is good for modeling purposes, it is not a good candidate for use in a real time system. Other types of neuronal activity such as LFP, EEG must be considered for adapting the stimulation parameters in real time. Thus modeling such signals and determining the effect of stimulation parameters on them is another interesting direction of future work.

The only dominant symptom in ET is kinetic tremor (tremor during voluntary movement), hence, sEMG/acc signals would be sufficient for tremor prediction. However, finding a relationship between the effect of stimulus on measured neuronal activity and sEMG/acc from the same patient will help determine if detectable changes in the neuronal activity immediately after stimulus is stopped corresponds to the no-tremor period. This would also help relating changes in model parameters from DBS-ON to DBS-OFF state with the reappearance of disease symptoms. Although, sEMG/acc can be used to detect an incoming tremor, neuronal activity can be used to determine optimal stimulation parameters and duration which can be updated in real time.

Use of multiple signals is more important for PD patients as PD symptoms are not limited to rest/kinetic tremor which can be detected by sEMG/acc. Other dominant PD symptoms

such as bradykinesia and rigidity cannot be detected by sEMG/acc alone and requires the measurement of neuronal activity. PD symptoms have been shown to be correlated with an increase in beta band (12-30 Hz) power in LFP measured from the STN of PD patients (27) and an increased firing rate in STN neurons (5; 13), both of which are reduced by DBS (7). Changes in such characteristics of neuronal activity could thus serve as a good metric for determining stimulus switching on time for an adaptive control. Thus combining both type of signals, ie signals measured from the brain and that measured non-invasively from the muscles would provide a more holistic understanding of the effect of stimulus on disease symptoms and will help design a more efficient adaptive ON-OFF DBS control algorithm.

CITED LITERATURE

1. Volkmann, J., Herzog, J., Kopper, F., and Deuschl, G.: Introduction to the programming of deep brain stimulators. Movement disorders, 17(S3):S181–S187, 2002.

2. Kringelbach, M., Jenkinson, N., Owen, S., and Aziz, T.: Translational principles of deep brain stimulation. Nature Reviews Neuroscience, 8(8):623–635, 2007.

3. Gildenberg, P.: Evolution of neuromodulation. Stereotactic and functional neurosurgery, 83(2-3):71–79, 2005.

4. de Lau, L. M. L. and Breteler, M.: Epidemiology of Parkinson's disease. The Lancet Neurology, 5(6):525–535, 2006.

5. Lozano, A. M., Dostrovsky, J., Chen, R., and Ashby, P.: Deep brain stimulation for parkinson's disease: disrupting the disruption. Lancet Neurol, 1(4):225–231, 2002.

6. Metman, L. V., Konitsiotis, S., and Chase, T. N.: Pathophysiology of motor response complications in parkinson's disease: hypotheses on the why, where, and what. Movement Disorders, 15(1):3–8, 2000.

7. Meissner, W., Leblois, A., Hansel, D., Bioulac, B., Gross, C., Benazzouz, A., and Boraud, T.: Subthalamic high frequency stimulation resets subthalamic firing and reduces abnormal oscillations. Brain, 128(10):2372, 2005.

8. Brown, P., Oliviero, A., Mazzone, P., Insola, A., Tonali, P., and Di Lazzaro, V.: Dopamine dependency of oscillations between subthalamic nucleus and pallidum in Parkinson's disease. Journal of Neuroscience, 21(3):1033, 2001.

9. Cameron C. McIntyre, Warren M. Grill, D. L. S. and Thakor, N. V.: Cellular effects of deep brain stimulation: Model-based analysis of activation and inhibition. Translational physiology, 2003.

10. McIntyre, C., Mori, S., Sherman, D., Thakor, N., and Vitek, J.: Electric field and stimulating influence generated by deep brain stimulation of the subthalamic nucleus. Clinical Neurophysiology, 115(3):589–595, 2004.

11. Vitek, J. L.: Mechanisms of deep brain stimulation: Excitation or inhibition (commentary). Movement Disorders, 17(3):S69S72, 2002.

12. Dostrovsky, J. O. and Lozano, A. M.: Mechanisms of deep brain stimulation. Movement Disorders, 17(3):S63S68, 2002.

13. McIntyre, C., Savasta, M., Kerkerian-Le Goff, L., and Vitek, J.: Uncovering the mechanism (s) of action of deep brain stimulation: activation, inhibition, or both. Clinical Neurophysiology, 115(6):1239–1248, 2004.

14. Liliana Garcia, Giampaolo D'Alessandro, B. B. and Hammond, C.: High-frequency stimulation in parkinson's disease: more or less? TRENDS in Neurosciences, 28(4), April 2005.

15. Cameron C. McIntyre, Marc Savasta, B. L. and Vitek, J. L.: How does deep brain stimulation work? present understanding and future questions. Clinical Neurophysiology, 21:40–45, 2004.

16. Benito-León, J. and Louis, E.: Clinical update: diagnosis and treatment of essential tremor. The Lancet, 369(9568):1152–1154, 2007.

17. Louis, E., Ottman, R., and Hauser, W.: How common is the most common adult movement disorder? Estimates of the prevalence of essential tremor throughout the world. Movement Disorders, 13(1):5–10, 1998.

18. Louis, E. and Vonsattel, J.: The emerging neuropathology of essential tremor. Movement disorders: official journal of the Movement Disorder Society, 23(2):174, 2008.

19. Deuschl, G. and Elble, R.: The pathophysiology of essential tremor. Neurology, 54(11 Suppl 4):S14, 2000.

20. Koller, W., Hristova, A., and Brin, M.: Pharmacologic treatment of essential tremor. Neurology, 54(11 Suppl 4):S30, 2000.

21. Pahwa, R., Lyons, K., Wilkinson, S., Carpenter, M., Troster, A., Searl, J., Overman, J., Pickering, S., and Koller, W.: Bilateral thalamic stimulation for the treatment of essential tremor. Neurology, 53(7):1447, 1999.

22. Shahzadi, S., Tasker, R., and Lozano, A.: Thalamotomy for essential and cerebellar tremor. Stereotactic and Functional Neurosurgery, 65(1-4):11–17, 1995.

23. Graupe, D., Basu, I., Tuninetti, D., Vannemreddy, P., and Slavin, K.: Adaptively controlling deep brain stimulation in essential tremor patient via surface electromyography . Neurological Research, 32(9):899–905, 2010.

24. Basu, I., Graupe, D., Tuninetti, D., and Slavin, K.: Stochastic modeling of the neuronal activity in the subthalamic nucleus and model parameter identification from Parkinson patient data. Biological Cybernetics, 103:273–283, 2010.

25. Basu, I., Tuninetti, D., Graupe, D., and Slavin, K.: Stochastic modeling of the neuronal activity in the thalamus of essential tremor patient. In 32nd Annual International Conference of the IEEE Engineering in Medicine and Biology Society. IEEE, 2010.

26. Tass, P.: Phase Resetting in Medicine and Biology: Stochastic Modeling and data Analysis. Springer, Berlin Heidelberg New York., 2007.

27. Gatev, P., Darbin, O., and Wichmann, T.: Oscillations in the basal ganglia under normal conditions and in movement disorders. Movement disorders, 21(10):1566–1577, 2006.

28. Elble, R.: Origins of tremor. Lancet, 355(9210):1113, 2000.

29. Levy, R., Hutchison, W., Lozano, A., and Dostrovsky, J.: Synchronized neuronal discharge in the basal ganglia of parkinsonian patients is limited to oscillatory activity. Journal of Neuroscience, 22(7):2855, 2002.

30. Slavin, K., Thulborn, K., Wess, C., and Nersesyan, H.: Direct visualization of the human subthalamic nucleus with 3T MR imaging. American Journal of Neuroradiology, 27(1):80, 2006.

31. Tass, P.: Desynchronizing double-pulse phase resetting and application to deep brain stimulation. Biological Cybernetics, 85(5):343–354, 2001.

32. Tass, P.: Effective desynchronization with a resetting pulse train followed by a single pulse. EPL (Europhysics Letters), 55:171, 2001.

33. Weinberger, M., Mahant, N., Hutchison, W., Lozano, A., Moro, E., Hodaie, M., Lang, A., and Dostrovsky, J.: Beta oscillatory activity in the subthalamic nucleus and its relation to dopaminergic response in Parkinson's disease. Journal of neurophysiology, 96(6):3248, 2006.

34. Elble, R.: Central mechanisms of tremor. Journal of Clinical Neurophysiology, 13(2):133, 1996.

35. Speelman, J., Schuurman, P., De Bie, R., and Bosch, D.: Thalamic surgery and tremor. Movement Disorders, 13(S3):103–106, 1998.

36. Boecker, H. and Brooks, D.: Functional imaging of tremor. Movement Disorders, 13(S3):64–72, 1998.

37. Halliday, D., Conway, B., Farmer, S., Shahani, U., Russell, A., and Rosenberg, J.: Coherence between low-frequency activation of the motor cortex and tremor in patients with essential tremor. The Lancet, 355(9210):1149–1153, 2000.

38. Hua, S., Lenz, F., Zirh, T., Reich, S., and Dougherty, P.: Thalamic neuronal activity correlated with essential tremor. Journal of Neurology, Neurosurgery & Psychiatry, 64(2):273, 1998.

39. Hellwig, B., Haubbler, S., Schelter, B., Lauk, M., Guschlbauer, B., Timmer, J., and Lucking, C.: Tremor-correlated cortical activity in essential tremor. The Lancet, 357(9255):519–523, 2001.

40. Volkmann, J., Joliot, M., Mogilner, A., Ioannides, A., Lado, F., Fazzini, E., Ribary, U., and Llinas, R.: Central motor loop oscillations in parkinsonian resting tremor revealed magnetoencephalography. Neurology, 46(5):1359, 1996.

41. Bar-Gad, I. and Bergman, H.: Stepping out of the box: information processing in the neural networks of the basal ganglia. Current Opinion in Neurobiology, 11(6):689–695, 2001.

42. Baltuch, G. H. and Stern, M. B.: Deep brain stimulation for Parkinson's disease.. CRC Press, 2007.

43. Feng, X. J., Greenwald, B., Rabitz, H., Shea-Brown, E., and Kosut, R.: Toward closed-loop optimization of deep brain stimulation for parkinsons disease: Concepts and lessons from a computational model. J. Neuroengineering, 4:L14–21, 2007.

44. Lee, J.: A Closed-Loop Deep Brain Stimulation Device With a Logarithmic Pipeline ADC. Doctoral dissertation, University of Michigan, 2008.

45. Schiff, S. J.: Towards model-based control of parkinson's disease. Philos Transact A Math Phys Eng Sci, 368(1918):2269–2308, 2010.

46. Hodgkin, A. and Huxley, A.: A quantitative description of membrane current and its application to conduction and excitation in nerve. The Journal of physiology, 117(4):500, 1952.

47. Humphries, M.: The basal ganglia and action selection: A computational study at multiple levels of description. 2002.

48. Humphries, M., Stewart, R., and Gurney, K.: A physiologically plausible model of action selection and oscillatory activity in the basal ganglia. The Journal of Neuroscience, 26:12921–12942, 2006.

49. Graupe, D.: Time series analysis, identification and adaptive filtering. RE Krieger Pub., 1984.

50. Kuffler, S. W., Fitzhugh, R., and Barlow, H. B.: Maintained activity in the cat's retina in light and darkness. J Gen Physiol., 40(5):683–702, 1957.

51. Grossman, R. G. and Viernstein, L. J.: Discharge patterns of neurons in cochlear nucleus. Science, 134(3472):99–101, 1961.

52. Gerstein, G. L. and Mandelbrot, B.: Random walk models for the spike activity of a single neuron. Biophysical Journal, 4:41–68, 1964.

53. Burns, B. D. and Webb, A. C.: The spontaneous activity of neurones in the cat's cerebral cortex. Proceedings of the Royal Society of London. Series B, Biological Sciences, 194(1115):211–223, 1976.

54. Sarma, S. V., Cheng, M., Hu, R., Williams, Z., Brown, E. N., and Eskandar, E.: Modeling neural spiking activity in the sub-thalamic nucleus of parkinson's patients and healthy primates. In Proceedings of the 17th World Congress The International Federation of Automatic Control, 2008.

55. Pasemann, F.: A simple chaotic neuron. Physica D: Nonlinear phenomena, 104(2):205–211, 1997.

56. Sarbaz, Y., Banaie, M., Golpayegani, M., Towhidkhah, F., Gharibzadeh, S., and Pooyan, M.: A Chaotic Viewpoint on DBS Treatment of Parkinson's Disease. Journal of Neuropsychiatry and Clinical Neurosciences, 22(2):247, 2010.

57. Uhlenbeck, G. and Ornstein, L.: On the theory of brownian motion. Phys.Rev, 36:823–841, 1930.

58. Gluss, B.: A model for neuron firing with exponential decay of potential resulting in diffusion equations for probability density. Bulletin of Mathematical Biophysics, 29:233–243, 1967.

59. Ricciardi, L. M. and Sacerdote, L.: The ornstein-uhlenbeck process as a model for neuronal activity i. mean and variance of the firing time. Biological Cybernetics, 35:1–9, 1979.

60. Capocelli, R. M. and Ricciardi, L. M.: Diffusion approximation and first passage time problem for a model neuron. Kybernetik, 8(6):214–223, 1971.

61. Shinomoto, S., Sakai, Y., and Funahashi, S.: The ornstein-uhlenbeck process does not reproduce spiking statistics of neurons in prefrontal cortex. Neural Computation, 11(4):935–951, 1999.

62. Hanson, F. and Westman, J.: Applied stochastic processes and control for Jump-diffusions: modeling, analysis, and computation. Citeseer, 2007.

63. Schuss, Z.: Diffusion and stochastic Processes.. Springer Verlag(in print), 2009.

64. Ricciardi, L. M. and Sato, S.: First-passage-time density and moments of the Ornstein-Uhlenbeck process. Journal of Applied Probability, 25(1):43–57, 1988.

65. Siegert, A.: On the first passage time probability problem. Physical Review, 81(4):617–623, 1951.

66. Israel, Z. and Burchiel, K.: Microelectrode recording in movement disorder surgery. Thieme Stuttgart, 2004.

67. Slavin, K. V. and Burchiel, K. J.: Microguide microelectrode recording system. Neurosurgery, 51:275–278, 2002.

68. Freedman, D. and Diaconis, P.: On the histogram as a density estimator: L 2 theory. Probability Theory and Related Fields, 57(4):453–476, 1981.

69. Inoue, J., Sato, S., and Ricciardi, L.: On the parameter estimation for diffusion models of single neuron's activities. Biological Cybernetics, 73:209–221, 1995.

70. Kandel, E. R., Schwartz, J. H., and Jessell, T. M.: Principles of neural science. McGraw-Hill/Appleton & Lange, 2000.

71. Buonocore, A., Nobile, A. G., and Ricciardi, L. M.: A new integral equation for the evaluation of first-passage-time probability densities. Advances in Applied Probability, 19(4):784–800, 1987.

72. Kullback, S. and Leibler, R.: On information and sufficiency. The Annals of Mathematical Statistics, 22(1):79–86, 1951.

73. Corder, G. W. and Foreman, D. I.: Nonparametric statistics for non-statisticians: A step-by-step approach. Wiley, 2009.

74. Cheng, R. C. H. and Amin, N. A. K.: Maximum likelihood estimation of parameters in the inverse gaussian distribution, with unknown origin. Technometrics, 23(3):257–263, 1981.

75. Santaniello, S., Fiengo, G., Glielmo, L., and Grill, W. M.: Closed-loop control of deep brain stimulation: A simulation study. Neural Systems and Rehabilitation Engineering, IEEE Transactions on, (99):1–1, 2011.

76. Dorval, A., Russo, G., Hashimoto, T., Xu, W., Grill, W., and Vitek, J.: Deep brain stimulation reduces neuronal entropy in the mptp-primate model of parkinson's disease. Journal of neurophysiology, 100(5):2807–2818, 2008.

77. Basu, I., Tuninetti, D., Graupe, D., and Slavin, K. V.: Adaptive control of deep brain stimulator for essential tremor: Entropy-based tremor prediction using surface-emg. In Conference proceedings:International Conference of the IEEE EMBC., page 7711, 2011.

78. Hua, S., Lenz, F., Zirh, T., Reich, S., and Dougherty, P.: Thalamic neuronal activity correlated with essential tremor. Journal of Neurology, Neurosurgery & Psychiatry, 64(2):273, 1998.

79. Pullman, S., Goodin, D., Marquinez, A., Tabbal, S., and Rubin, M.: Clinical utility of surface EMG: report of the therapeutics and technology assessment subcommittee of the American Academy of Neurology. Neurology, 55(2):171, 2000.

80. Hogrel, J.: Clinical applications of surface electromyography in neuromuscular disorders. Neurophysiologie Clinique/Clinical Neurophysiology, 35(2-3):59–71, 2005.

81. Graupe, D., Salahi, J., and Zhang, D. S.: Stochastic analysis of myoelectric temporal signatures for multifunctional single-site activation of prostheses and orthoses. Journal of biomedical engineering, 7(1):18–29, 1985.

82. Graupe, D., Kohn, K., and Basseas, S.: Above-and below-lesion EMG pattern mapping for controlling electrical stimulation of paraplegics to facilitate unbraced walker-assisted walking. Journal of biomedical engineering, 10(4):305–311, 1988.

83. Waxman, J., Graupe, D., and Carley, D.: Automated Prediction of Apnea and Hypopnea, Using a LAMSTAR Artificial Neural Network. American journal of respiratory and critical care medicine, 181(7):727, 2010.

84. Serridge, M. and Licht, T. R.: Piezoelectric accelerometer and vibration preamplifier handbook. Brüel & Kjaer, 1987.

85. Piezotronics, P. C. B.: Sensing technologies used for accelerometers. http://www.pcb.com/Accelerometers/Sensing_Technologies.asp.

86. Vaillancourt, D., Sturman, M., Verhagen Metman, L., Bakay, R., and Corcos, D.: Deep brain stimulation of the VIM thalamic nucleus modifies several features of essential tremor. Neurology, 61(7):919, 2003.

87. Morrison, S. and Newell, K. M.: Postural and resting tremor in the upper limb. Clinical neurophysiology, 111(4):651–663, 2000.

88. Leondopulos, S. S. and Micheli-Tzanakou, E.: Advances toward closed-loop deep brain stimulation. Computational Neuroscience, pages 227–253, 2010.

89. Popovych, O. V., Hauptmann, C., and Tass, P. A.: Control of neuronal synchrony by nonlinear delayed feedback. Biological cybernetics, 95(1):69–85, 2006.

90. Rosin, B., Slovik, M., Mitelman, R., Rivlin-Etzion, M., Haber, S. N., Israel, Z., Vaadia, E., and Bergman, H.: Closed-loop deep brain stimulation is superior in ameliorating parkinsonism. Neuron, 72(2):370–384, 2011.

91. Hauptmann, C., Roulet, J. C., Niederhauser, J. J., Döll, W., Kirlangic, M. E., Lysyansky, B., Krachkovskyi, V., Bhatti, M. A., Barnikol, U. B., Sasse, L., et al.: External trial deep brain stimulation device for the application of desynchronizing stimulation techniques. Journal of neural engineering, 6:066003, 2009.

92. Farina, D., Fattorini, L., Felici, F., and Filligoi, G.: Nonlinear surface EMG analysis to detect changes of motor unit conduction velocity and synchronization. Journal of Applied Physiology, 93(5):1753, 2002.

93. Rosso, O. A., Blanco, S., Yordanova, J., Kolev, V., Figliola, A., Schurmann, M., and Basar, E.: Wavelet entropy: a new tool for analysis of short duration brain electrical signals. Journal of neuroscience methods, 105(1):65–75, 2001.

94. Zelmann, R., Mari, F., Jacobs, J., Zijlmans, M., Chander, R., and Gotman, J.: Automatic detector of High Frequency Oscillations for human recordings with macroelectrodes. In EMBC 2010, Annual International Conference of the IEEE, pages 2329–2333. IEEE, 2010.

95. Jayachandran, E. S., Joseph K, P., and Acharya U, R.: Analysis of myocardial infarction using discrete wavelet transform. Journal of medical systems, pages 1–8, 2010.

96. Ocak, H.: Automatic detection of epileptic seizures in EEG using discrete wavelet transform and approximate entropy. Expert Systems with Applications, 36(2):2027–2036, 2009.

97. Pincus, S. M. and Goldberger, A. L.: Physiological time-series analysis: what does regularity quantify? American Journal of Physiology-Heart and Circulatory Physiology, 266(4):H1643, 1994.

98. Richman, J. S. and Moorman, J. R.: Physiological time-series analysis using approximate entropy and sample entropy. American Journal of Physiology-Heart and Circulatory Physiology, 278(6):H2039, 2000.

99. Shannon, C. E.: A mathematical theory of communication. ACM SIGMOBILE Mobile Computing and Communications Review, 5(1):3–55, 2001.

100. Semmler, J. G. and Nordstrom, M. A.: A comparison of cross-correlation and surface emg techniques used to quantify motor unit synchronization in humans. Journal of neuroscience methods, 90(1):47–55, 1999.

101. Filligoi, G. and Felici, F.: Detection of hidden rhythms in surface EMG signals with a non-linear time-series tool. Medical engineering & physics, 21(6-7):439–448, 1999.

102. Webber Jr, C. and Zbilut, J.: Recurrence quantification analysis of nonlinear dynamical systems. Tutorials in contemporary nonlinear methods for the behavioral sciences, pages 33–101, 2005.

103. Marwan, N., Carmen Romano, M., Thiel, M., and Kurths, J.: Recurrence plots for the analysis of complex systems. Physics Reports, 438(5-6):237–329, 2007.

104. Sturman, M. M., Vaillancourt, D. E., Verhagen-Metman, L., Bakay, R. A. E., and Corcos, D. M.: Effects of subthalamic nucleus stimulation and medication on resting and postural tremor in parkinson's disease. Brain, 127(9):2131–2143, 2004.

105. Pincus, S. M.: Approximate entropy as a measure of system complexity. Proceedings of the National Academy of Sciences of the United States of America, 88(6):2297–2301, 1991.

106. Marwan, N.: Toolboxes for complex systems. http://tocsy.pik-potsdam.de/index2.php.

107. Baldi, P., Brunak, S., Chauvin, Y., Andersen, C., and Nielsen, H.: Assessing the accuracy of prediction algorithms for classification: an overview. Bioinformatics, 16(5):412–424, 2000.

108. Temperli, P., Ghika, J., Villemure, J. G., Burkhard, P. R., Bogousslavsky, J., and Vingerhoets, F. J. G.: How do parkinsonian signs return after discontinuation of subthalamic dbs? Neurology, 60(1):78–81, 2003.

109. Pilitsis, J. G., Metman, L. V., Toleikis, J. R., Hughes, L. E., Sani, S. B., and Bakay, R. A. E.: Factors involved in long-term efficacy of deep brain stimulation of the thalamus for essential tremor. Journal of neurosurgery, 109(4):640–646, 2008.

110. Kumar, R., Lozano, A. M., Sime, E., and Lang, A. E.: Long-term follow-up of thalamic deep brain stimulation for essential and parkinsonian tremor. Neurology, 61(11):1601–1604, 2003.

111. Graupe, D.: Principles of artificial neural networks, volume 6. World Scientific Pub Co Inc, 2007.

VITA

NAME	Ishita Basu
EDUCATION	B.S., Instrumentation & Electronics Engineering, Jadavpur University, Kolkata, India, 2005
	M.S.,Electrical & Computer Engineering, University of Illinois at Chicago, Chicago, Illinois, 2010
	M.S.,Applied Mathematics, University of Illinois at Chicago, Chicago, Illinois, 2011
	Ph.D.,Electrical & Computer Engineering, University of Illinois at Chicago, Chicago, Illinois, 2012
RESEARCH	Research Assistant in department of Electrical & Computer Engineering, University of Illinois at Chicago, 2007–2012
	Summer intern in Biomedical Image Processing Lab, EPFL, Switzerland, 2009
TEACHING	Adjunct Lecturer in department of Electrical & Computer Engineering, University of Illinois at Chicago, Summer 2012
	Teaching Assistant in department of Electrical & Computer Engineering, University of Illinois at Chicago, 2007–2010
OTHER EXPERIENCE	Graduate Assistant at JSC Global Solutions, Naperville, Illinois, 2007
	Software Engineer at Infosys Technologies, Pune, India, 08/2005–08/2006

HONORS

FMC Educational Fund fellowship, University of Illinois at Chicago, 2008-09

Thinkswiss Research Fellowship, 2009

Chancellor's Supplemental Graduate Research Fellowship, University of Illinois at Chicago, 2010.

Deans Scholar Award, University of Illinois at Chicago, 2011-12.

SKILLS

Extensive knowledge of MATLAB, Simulink.

Experience of C, C++ programming.

Working knowledge of LaTeX.

MEMBERSHIPS

Student member of IEEE engineering in Medicine and Biology society.

Student member of the honor society of Phi Kappa Phi.

PUBLICATIONS

Basu,I., Graupe,D., Tuninetti,D., Shukla,P., Verhagen L.M., Slavin,K.V., and Corcos,D.M.: Closed loop adaptive control of Deep Brain Stimulator for Pathological Tremor. IEEE transactions in neural systems engineering and rehabilitation(submitted)

Basu,I., Graupe,D., Tuninetti,D., and Slavin,K.V.: Stochastic modeling of the neuronal activity in the subthalamic nucleus and model parameter identification from Parkinson patient data. Biological Cybernetics. 103(4): 273–83, 2010.

Graupe,D., Basu,I., Tuninetti,D., Vannemreddy,P., and Slavin,K.V.: Adaptively controlling deep brain stimulation in essential tremor patient via surface electromyography. Neurological Research. 32(9): 899-904, 2010.

Acharya,K., Mazumder,S.K., and Basu,I.: Reaching Criterion of a Three-phase Voltage Source Inverter Operating with Passive and Nonlinear Loads and its Impact on Global Stability. IEEE transaction on Industrial Electronics. 55(4), 2008.

CONFERENCE PROC.

Basu,I., Tuninetti,D., Graupe,D., and Slavin,K.V.: A model for simulating Local Field Potential in the thalamus of Essential Tremor patient during deep brain stimulation. 21st Annual Computational Neuroscience Meeting. 2012.

Shukla,P., Basu,I., Graupe,D., Tuninetti,D., and Slavin,K.V.: Neural Network-based Design of an Adaptive on-off control for Deep Brain Stimulation in Movement Disorders. 34th IEEE EMBC. 2012.

Basu,I., Tuninetti,D., Graupe,D., and Slavin,K.V.: Adaptive Control of Deep Brain Stimulator for Essential Tremor:Entropy-based Tremor Prediction Using Surface-EMG. 33rd IEEE EMBC. 2011.

Graupe,D., Basu,I., Tuninetti,D., and Slavin,K.V.: Relating thalamic neuronal activity and EMG for validating predictive control of deep-brain stimulation in Essential Tremor patients. 20th Annual Computational Neuroscience Meeting. 2011.

Basu,I., Tuninetti,D., Graupe,D., and Slavin,K.V.: Stochastic Modeling of the Neuronal Activity in the Thalamus of Essential Tremor patient. 32nd IEEE EMBC. 2010.

REFERENCES

Prof. Tuninetti, Daniela, email: danielat@uic.edu

Prof. Graupe, Daniel, email: dangraupe@gmail.com

Dr. Slavin, Konstantin V., email: kslavin@uic.edu